Published in : Earth and Planetary Science Letters (2024), vol. 646, 118989
DOI: 10.1016/j.epsl.2024.118989
Status : Postprint (Author's version)

THE VERY LATE-STAGE CRYSTALLIZATION OF THE LUNAR MAGMA OCEAN AND THE COMPOSITION OF IMMISCIBLE URKREEP

Yishen Zhang

Department of Earth and Environmental Sciences, KU Leuven, 3001 Leuven, Belgium – Department of Earth, Environmental and Planetary Sciences, Rice University, 6100 Main Street, MS 126, Houston, TX 77005, USA

Bernard Charlier

Department of Geology, University of Li`ege, 4000 Sart Tilman, Belgium – Massachusetts Institute of Technology, Department of Earth, Atmospheric, and Planetary Sciences, Cambridge, MA 02139 USA – Institut für Erdsystemwissenschaften, IESW, Abteilung Mineralogie, Leibniz Universitat¨ Hannover, 30167 Hannover (Germany).

Stephanie B. Krein

Massachusetts Institute of Technology, Department of Earth, Atmospheric, and Planetary Sciences, Cambridge, MA 02139 (USA).

Timothy L. Grove

Massachusetts Institute of Technology, Department of Earth, Atmospheric, and Planetary Sciences, Cambridge, MA 02139 (USA).

Olivier Namur

Department of Earth and Environmental Sciences, KU Leuven, 3001 Leuven, Belgium – Institut für Erdsystemwissenschaften, IESW, Abteilung Mineralogie, Leibniz Universitat¨ Hannover, 30167 Hannover (Germany).

Francois Holtz

Institut für Erdsystemwissenschaften, IESW, Abteilung Mineralogie, Leibniz Universitat¨ Hannover, 30167 Hannover (Germany).

Abstract. The latest stages of the lunar magma ocean (LMO) crystallization led to the formation of ilmenite-bearing cumulates and urKREEP, residual melts enriched in K, rare earth elements (REEs), P, and other incompatible elements. Those highly evolved lithologies had major impacts on the petrogenesis of lunar volcanic rocks and the compositional diversity of post-LMO magmatism resulting from mantle remelting. Here, we present new experimental results constraining the composition of the very last liquids produced during LMO crystallization. To test the potential role of silicate liquid immiscibility in the formation of urKREEP, synthetic samples representative of residual melts of bulk Moon compositions were placed in double platinum-graphite capsules at 1020–980 °C and 0.08–0.10 GPa in an internally-heated pressure vessel. The produced silicate liquids

Published in : Earth and Planetary Science Letters (2024), vol. 646, 118989
DOI: 10.1016/j.epsl.2024.118989
Status : Postprint (Author's version)

are multiply saturated with plagioclase, augite, silica phases, and ilmenite (± fayalitic olivine ± pigeonite). Our experiments show that the liquid line of descent reaches a two-liquid field at 1000 °C and >97% crystallization for a range of whole-Moon compositions. Under these conditions, a small proportion of silica-rich melt (70.0–71.4 wt.% SiO_2, 6.4–7.3 wt.% FeO, 5.4–6.1 wt.% K_2O, 0.2–0.3 wt.% P_2O_5) coexists within an abundant Ferich melt (42.6–44.1 wt.% SiO_2, 27.6–28.8 wt.% FeO, 0.9–1.0 wt.% K_2O, 2.8–3.2 wt.% P_2O_5) with sharp twoliquid interfaces. Our experimental results also constrain the relative onset of ilmenite crystallization compared to the development of immiscibility and indicate that an ilmenite-bearing layer formed in the lunar interior before immiscibility was attained. Using a self-consistent physicochemical LMO model, we constrain the thickness and depth of the ilmenite-bearing layer during LMO differentiation. The immiscible K-Si-rich and P-Ferich melts together also produced an immiscible urKREEP layer ~2–6 km thick and ~30–50 km deep depending on the trapped liquid fraction in the cumulate column (≤10%) and the thickness of the buoyant anorthosite crust (30–50 km). We provide constraints on the relationship between the compositions of immiscible urKREEP melts and those of KREEPy rocks. By modeling the mixing of KREEP-poor basalt and the immiscible melt pairs, we reproduce the K and P enrichments and apparent decoupling of K from P in KREEPy rocks. Our results highlight that processes such as the assimilation of evolved heterogeneous mantle lithologies may be involved in hybridization during post-LMO magmatism. The immiscible K-Si-rich lithology may also have contributed to lunar silicic magmatism.

Keywords. KREEP basalt, Differentiation, Liquid immiscibility, Ilmenite, Lunar magma ocean.

1. Introduction

Material ejected during a giant impact between proto-Earth and another planetary body is thought to have formed the Moon around 4.5–4.3 Ga (Cameron and Ward, 1976; Canup, 2012), which was initially covered by the lunar magma ocean (LMO; Tonks and Melosh, 1993; Kleine et al., 2005; Elkins-Tanton, 2012; Gaffney and Borg, 2014). Cooling and crystallization of the LMO formed distinct primordial mantle and crustal layers (Smith et al., 1970; Wood et al., 1970; Taylor and Jakeˇs, 1974), eventually producing residual melts strongly enriched in incompatible elements. These last dregs of magmas were termed urKREEP because of their enrichment in K, rare earth elements (REEs), P, and other incompatible elements (Warren and Wasson, 1979; the German prefix 'ur-' meaning 'primeval'). Although urKREEP has never been identified as a pristine rock-type on the lunar surface, it is recognized as a chemical component in a range of lunar lithologies, i.e. the 'KREEP signature'. Rocks with KREEP signatures are termed 'KREEPy' or 'KREEP-rich' rocks (hereafter, we use KREEPy). KREEPy rocks include magnesian troctolites (Mg-suite rocks), picritic glasses, impact-melt breccias, mare basalts, lunar soils, and highland rocks (e.g., Ryder et al., 1977; Warren and Wasson, 1979; Warren, 1988; Shervais and McGee, 1998). Remote sensing and geophysical data indicate a crustal province on the Moon's nearside with elevated Th abundances and heat flow, consistent with an abundance of KREEP-like materials, i.e. the Procellarum KREEP Terrane (PKT; Jolliff et al., 2000; Korotev, 2000; Wieczorek and Phillips, 2000; Qian et al., 2023). Areas within the PKT also contain elevated REE abundances (Elphic et al., 2000).

Published in : Earth and Planetary Science Letters (2024), vol. 646, 118989
DOI: 10.1016/j.epsl.2024.118989
Status : Postprint (Author's version)

The petrogenesis and composition of the most evolved melts produced during LMO crystallization have important implications for the volatile budget of the lunar interior (McCubbin et al., 2011, 2015; Pernet-Fisher et al., 2014; Robinson et al., 2016; Barnes et al., 2016; Greenwood et al., 2017). Heat-producing elements (K, U, Th) are also enriched in residual melts, so these processes also impacted the thermal evolution of the Moon (Solomon and Longhi, 1977; Hess and Parmentier, 1995, 2001; Tosi and Padovan, 2021) and potentially the development of the dichotomy between mare basalts and highlands on the lunar surface (Parmentier et al., 2002; Laneuville et al., 2013). The urKREEP reservoir and KREEP component are also important to the petrogenesis of lunar granites, such as those found in Apollo samples (Drake et al., 1970; Zhang et al., 2012; Seddio et al., 2013), and most probably the formation of silicic compositions identified remotely on the lunar surface (Hagerty et al., 2006; Glotch et al., 2010, 2011; Jolliff et al., 2011). During its late-stage evolution, the LMO became saturated in ilmenite, which resulted in the formation of a dense, gravitationally unstable, ilmenite-bearing cumulate layer (IBL or Fe-Ti-rich KREEP layer) that may have led to the overturn of the lunar mantle (Kesson and Ringwood, 1976; Hess and Parmentier, 1995; Elkins-Tanton et al., 2002; Parmentier et al., 2002; Dygert et al., 2016; Zhang et al., 2017; Li et al., 2019; Xu et al., 2022; Yu et al., 2019; Maurice et al., 2024).

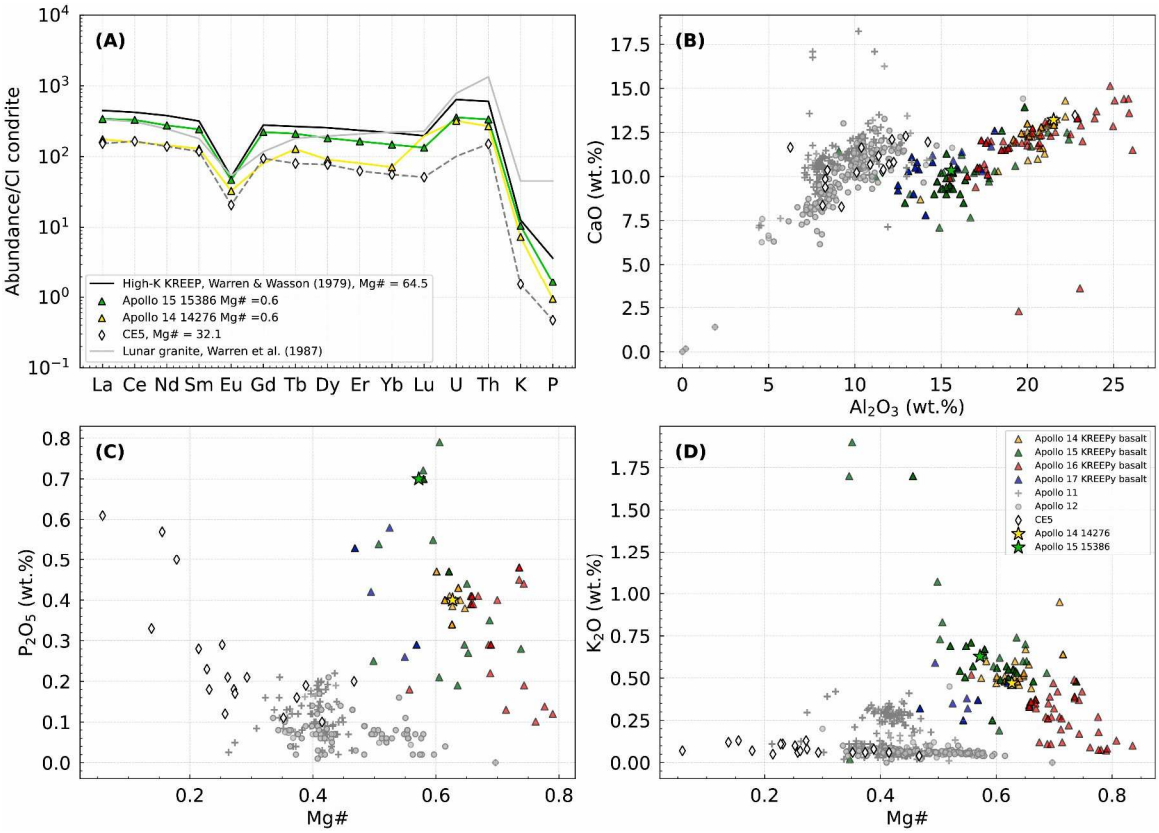

Fig. 1. Geochemistry of KREEPy and non-KREEPy basalts. (A) Chondrite-normalized abundances of heat producing elements (K, U, Th), P, and REEs in a high-K KREEP basalt (Warren and Wasson, 1979), representative KREEPy basalts returned by Apollo 15 (15,386) and Apollo 14 (14,276) (data source: Clive Neal's Mare Basalt Database; https://www3.nd.edu/~cneal/Lunar-L/), and non-KREEPy rocks (Chang'E 5 ferrobasalt, CE5, Tian et al., 2021; and

Published in : Earth and Planetary Science Letters (2024), vol. 646, 118989
DOI: 10.1016/j.epsl.2024.118989
Status : Postprint (Author's version)

a lunar granite, Warren et al., 1987). (B) CaO vs. Al_2O_3 contents (C) P_2O_5 content vs. Mg#, and (D) K_2O content vs. Mg# in lunar basalts. In (B–D), colored symbols are KREEPy basalts selected from the Mare Basalt Database for their high concentrations of K, REEs, P, and other incompatible elements and isotopic signatures (e.g., Rb-Sr isotopes; Nyquist et al., 1973; Nyquist, 1977); gray symbols (Apollo 11, Apollo 12, and CE5) are non-KREEPy basalts

Our understanding of the evolution of the LMO has advanced greatly thanks to crystallization modeling (Snyder et al., 1992; Elkins-Tanton et al., 2011) and experiments on bulk lunar compositions and their derivative liquids (Elardo et al., 2011; Lin et al., 2017a, 2017b; Charlier et al., 2018; Rapp and Draper, 2018; Kraettli et al., 2022; Schmidt and Kraettli, 2022). However, the origin of urKREEP and KREEPy rocks remains debated, with the current leading hypothesis being that urKREEP resulted from extreme fractional crystallization of the LMO (Warren and Wasson, 1979; Snyder et al., 1992; Charlier et al., 2018; Jing et al., 2022). During this process, the pronounced incompatibilities of K, P, and REEs led to their continuous enrichment in the melt, reaching extremely high values during the latest stages of evolution; for example, for an initial LMO containing 0.04 wt.% K_2O and chondrite-normalized REE abundances of 3, the residual melt reaches ~4 wt.% K_2O and REE abundances ~400 times those in Cl chondrites at 99% solidification (PCS; Hughes et al., 1988; Snyder et al., 1992). Interestingly, KREEPy rocks exhibit chemical characteristics of both primitive (e.g., high Mg#= Mg / [Mg + Fe]) and evolved magmas (e.g., their namesake enrichments in K, P, REEs, and trace elements; Fig. 1). They also have lower CaO and higher Al_2O_3 contents compared to non-KREEPy basalts (e.g., Apollo 11 and 12 rocks), reflecting their lower modal abundances of Ca-rich pyroxene (Fig. 1). These unique characteristics are often attributed to processes such as the remelting of the lunar interior followed by assimilation of the urKREEP lithology during upwards melt migration (Warren and Wasson, 1979; Snyder et al., 1992), impact-induced mixing of shallow KREEP-rich material with deeper, primitive lithologies (McKay et al., 1979), or crystallization from KREEP-enriched Mg-suite parental magmas that originate from hybridized mantle sources (Shearer and Papike, 2005). We note that Mg suite parental magma would not produce a KREEP basalt. However, these models fail to explain the decoupling of K from REE + P (REEP; see details in the Supplementary Material) in compositions enriched in REEP but highly depleted or enriched in K (Neal and Taylor, 1989; Jerde et al., 1994; Jolliff, 1998; Lin et al., 2012).

Experimental studies indicate that the residual liquids produced during the late stages of lunar differentiation exhibit ferrobasaltic compositions marked by extreme iron enrichments after plagioclase saturation, together with calcium, alumina, and magnesium depletions (Lin et al., 2017a, 2017b; Charlier et al., 2018; Rapp and Draper, 2018; Schmidt and Kraettli, 2022). Silicate liquid immiscibility—the separation of iron-rich and silica-rich melts—was proposed to develop very late during primordial lunar differentiation (Hess et al., 1975; Longhi, 1990). If so, this immiscibility is particularly relevant to the genesis of urKREEP because K tends to partition into the Si-rich melt, whereas REE and P preferentially partition into the Fe-rich melt (Watson, 1976; Schmidt et al., 2006; Veksler et al., 2006). The coexistence of high-viscosity silica-rich melts and low-viscosity iron-rich melts could hypothetically produce a urKREEP-like composition characterized by a range of K and REEP concentrations. However, such immiscibility develops late during differentiation, typically at <1020 °C, below the temperature range explored by experimental studies on LMO fractionation thus far (Lin et al., 2017a; Rapp and Draper, 2018; Charlier et al., 2018).

Published in : Earth and Planetary Science Letters (2024), vol. 646, 118989
DOI: 10.1016/j.epsl.2024.118989
Status : Postprint (Author's version)

Table 1
Normalized starting material compositions.

Sample No.[a]	SiO_2	TiO_2	Al_2O_3	Cr_2O_3	FeO	MnO	MgO	CaO	Na_2O	K_2O	P_2O_5	Sum
ON/02–3	49.32	1.55	11.08	0.09	23.01	0.35	3.20	10.70	0.31	0.12	0.27	100
ON/04–1.5	47.54	2.59	8.57		28.17	0.43	1.29	10.32	0.36	0.24	0.49	100
TWM/02–3	47.66	2.99	10.72	0.09	22.85	0.35	3.63	11.03	0.27	0.14	0.27	100
TWM/04–1.5	46.29	4.75	8.47		27.13	0.43	1.54	10.37	0.28	0.27	0.47	100
LPUM/02–3	47.58	4.27	10.78	0.09	21.39	0.22	3.80	10.94	0.51	0.14	0.27	100
LPUM/04–1.5	48.09	4.19	8.67		25.65	0.28	1.61	10.11	0.56	0.29	0.55	100

[a] Residual melt compositions from Charlier et al. (2018).

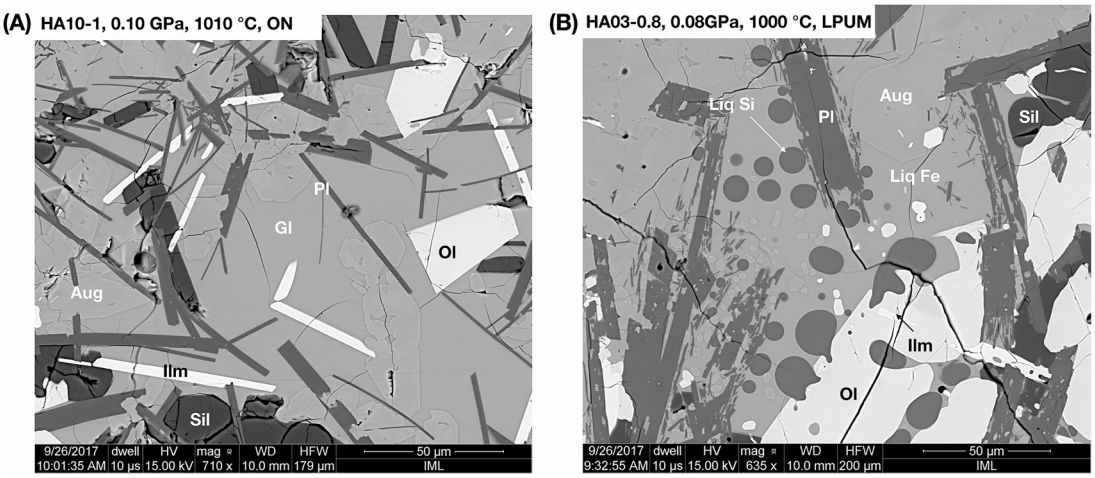

Fig. 2. Backscattered electron images of typical experimental products. (A) Experimental glass of ON composition at 1010 ˚C and 0.10 GPa, coexisting with plagioclase, augite, a silica phase, and olivine. (B) Experiment of LPUM composition at 1000 ˚C and 0.08 GPa showing silicate liquid immiscibility, containing Fe-rich melt cosaturated with Si-rich droplets. Abbreviations: Liq Fe, immiscible iron-rich glass; Liq Si, immiscible silica-rich glass; Ol, olivine; Pl, plagioclase; Aug, augite; Sil, silica phase (tridymite or β-quartz); Ilm, ilmenite.

In this study, we tested whether silicate liquid immiscibility could have developed late during LMO crystallization and, if so, whether it could have produced urKREEP melts. We also investigated whether such immiscible urKREEP melts might have controlled the geochemical signature of KREEPy rocks. To do this, we experimentally investigated the compositional evolution of very late-stage liquids produced during crystallization of the LMO at <1020 ˚C. Our experiments show that immiscibility occurs at around 1000 ˚C during the crystallization of a range of bulk lunar compositions after 97 PCS. Based on our results, we constrain the major element compositions of the K-rich and P-rich fractions of immiscible urKREEP melts and the K and P contents of their pre-immiscibility counterparts. Using a self-consistent physicochemical LMO model, we map the thickness and depth of the immiscible urKREEP layer, as well as the onset of ilmenite crystallization. We then finally discuss the K and REEP enrichments in KREEPy lunar rocks, the relation between the compositions of immiscible urKREEP melts and the KREEP signature, potential processes responsible for hybridization of post-LMO lithologies, and the contribution of late LMO immiscibility to lunar silicic magmatism.

Published in : Earth and Planetary Science Letters (2024), vol. 646, 118989
DOI: 10.1016/j.epsl.2024.118989
Status : Postprint (Author's version)

2. Methodology

2.1. EXPERIMENTAL STRATEGY

Our experiments aim to simulate the very late-stage evolution of the LMO during cooling. The first stage of crystallization (1500–1020 °C, up to ~97% crystallization) was presented in Charlier et al. (2018), and further steps of crystallization from 1020 °C down to 980 °C are presented herein. For our starting compositions, we used the compositions of residual melts produced at 1040 °C and 1020 °C for three bulk Moon compositions: the O'Neill (1991) bulk Moon composition ('ON'), the Taylor (1982) whole Moon ('TWM'), and the lunar primitive upper mantle (LPUM; Longhi, 2006) (Table 1). These starting compositions are globally in the same compositional field as late-stage LMO melts produced in other experimental studies (Lin et al., 2017a; Rapp and Draper, 2018).

2.2. STARTING MATERIALS AND EXPERIMENTAL TECHNIQUES

Starting synthetic compositions were prepared by mixing high purity oxides and silicates. We used SiO_2, TiO_2, Al_2O_3, Cr_2O_3, MnO, MgO, $CaSiO_3$, Na_2SiO_3, and $K_2Si_4O_9$ in the appropriate proportions. Iron was added as Fe_2O_3 and Fe metal sponge in stoichiometric proportions to produce the target FeO contents. Reagents were mixed under ethanol in an agate mortar for 5 h. The Fe sponge was then added to the mixture and ground for an additional hour. The mixtures were conditioned at 1 atm in a DelTech vertical gas-mixing furnace for 24–48 h at the Fe–FeO oxygen fugacity buffer at 950 °C.

Medium pressure experiments at 0.10 and 0.08 GPa and 1020–980 °C were conducted in an internally heated pressure vessel at the Leibniz University of Hannover (Berndt et al., 2002). Pure Ar gas was used as the pressure medium. Experiments were run using a double capsule technique with ~50 mg of starting powder sealed inside a graphite capsule (2.5 mm inner diameter) enclosed within a Pt jacket (4 mm inner diameter). The large volume and length of the hotspot (~2.5 cm) in these experiments allowed us to run up to three capsules simultaneously. The vessel was pressurized cold to the target pressure, then heated isobarically. Pressure was measured with a pressure transducer (±5 MPa accuracy). Experiments were heated by 30 °C/min up to 100 °C, then by 50 °C/min until 30 °C below the final temperature. At that point, the temperature was held constant for 2 min before heating to the final temperature at 20 °C/min. Temperature was controlled using two type-S thermocouples (Pt–$Pt_{90}Rh_{10}$) connected to a Eurotherm controller to regulate the power supply to the two furnace windings. Two additional type-S thermocouples at the bottom and top of the samples were used to monitor the actual temperature of the sample; the temperature gradient across the sample was generally less than 5 °C. The temperature distribution across all thermocouples was recorded at 1 s increments; in most experiments, temperature oscillated by less than 3 °C. Experiments were quenched by fusing the Pt wire on which the capsules were attached, dropping the capsules onto a cold copper block placed at the bottom of the water-cooled sample holder. Quench rates are estimated to be ca. 150 °C/s (e.g., Benne and Behrens, 2003).

Published in : Earth and Planetary Science Letters (2024), vol. 646, 118989
DOI: 10.1016/j.epsl.2024.118989
Status : Postprint (Author's version)

2.3. ANALYTICAL METHODS

Experimental charges were analyzed with a Cameca SX-100 electron microprobe at the Leibniz University of Hannover. Glasses were measured with a 15 kV and 8 nA beam with a spot size of 10 μm in most experiments. Peak counting times were 20 s for major elements and 40 s for minor elements, background counting times were half as peak counting times. Minerals were measured with a focused (1 μm diameter) 15 kV and 15 nA beam, with peak counting times of 20 s and background times as half for each element. The following standards were used for Kα X-ray line calibration of glasses and minerals: wollastonite for Si and Ca, TiO_2 for Ti, Al_2O_3 for Al, Fe_2O_3 for Fe, Mn_3O_4 for Mn, MgO for Mg, albite for Na, orthoclase for K, and Cr_2O_3 for Cr. Raw data were corrected with the CATZAF software. The complete mineral and glass dataset is reported in Supplementary Dataset Table S1.

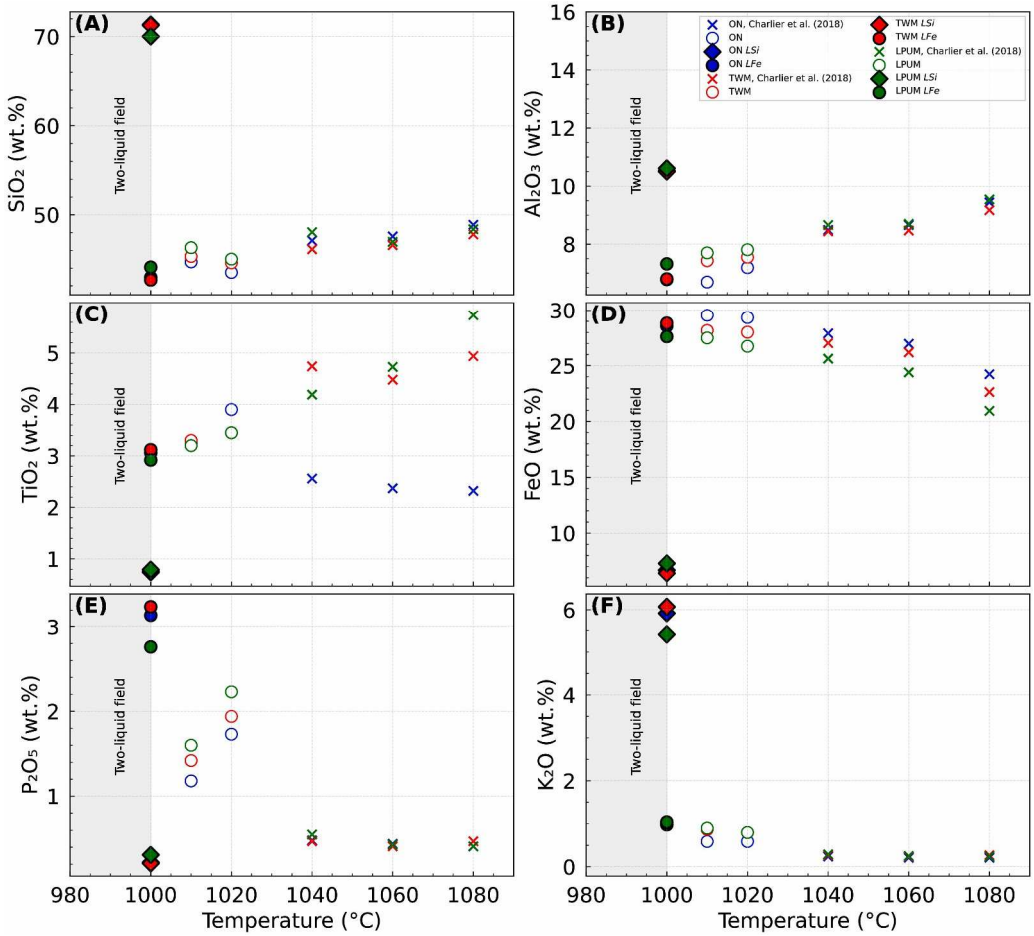

Fig. 3. Selected major element concentrations in the melt as a function of experimental temperature. '×' symbols are high temperature experiments from Charlier et al. (2018). The gray field indicates the field of silicate liquid immiscibility. Blue, red, and green symbols indicate the melt trajectories of the ON, TWM, and LPUM compositions, respectively.

Published in : Earth and Planetary Science Letters (2024), vol. 646, 118989
DOI: 10.1016/j.epsl.2024.118989
Status : Postprint (Author's version)

2.4. FRACTIONAL CRYSTALLIZATION MODELING

We modeled fractional crystallization as:

$$c^0_{i,Liq} = (1-z) \times c^1_{i,Liq} + z\left[\left(\sum_{j=1\to n} X^j c^j_i\right) \times X^{Mush}_{Sol} + c^0_{i,Liq} X^{Mush}_{Liq}\right] \quad (1)$$

Here z is the crystallization increment (fixed at 1%), which we scaled to account for mass conservation by recalculating the remaining mass of the liquid at each crystallization step. $c^1{}_{i,Liq}$ is the concentration of element i in the liquid at each crystallization step, $c^0{}_{i,Liq}$ is that in the liquid at the previous crystallization step, $c^j{}_i$ is the concentration of element i in the jth of n crystalline phases, X^j is the proportion of phase j in the cumulus assemblage, $X_{Sol}{}^{Mush}$ is the bulk proportion of solids in the crystal + trapped liquid mush, and $X_{Liq}{}^{Mush}$ is the proportion of trapped liquid in the crystal + liquid mush. Major element modeling during early crystallization steps was presented in Charlier et al. (2018).

2.5. LMO MODEL

The temperature, pressure, density, and gravity profiles of the residual liquid in a magma ocean change during crystallization. To account for these variations, we use a spherically symmetrical model (e.g., Rivoldini et al., 2009; Knibbe and van Westrenen, 2015) to construct the interior structure and corresponding profiles of the LMO, which depends on the radial distance to the center r. Hydrostatic equilibrium in the Moon is assumed to be:

$$P(r) = \int_r^R g(x)\rho(x)dx \quad (2)$$

The gravity (g, m/s^2), pressure (P, GPa), and density (ρ, kg/m^3) profiles can then be consecutively calculated from the Moon's surface toward its center in steps of 1 km by iteratively solving Eqs. (3), (4), and (2):

$$M(r) = M(R) - 4\pi \int_r^R \rho(x)x^2dx \quad (3)$$

$$g(r) = \frac{GM(r)}{r^2} \quad (4)$$

where G is the universal gravitational constant, R the radius at the surface, and M the mass within radius r or R.

Published in : Earth and Planetary Science Letters (2024), vol. 646, 118989
DOI: 10.1016/j.epsl.2024.118989
Status : Postprint (Author's version)

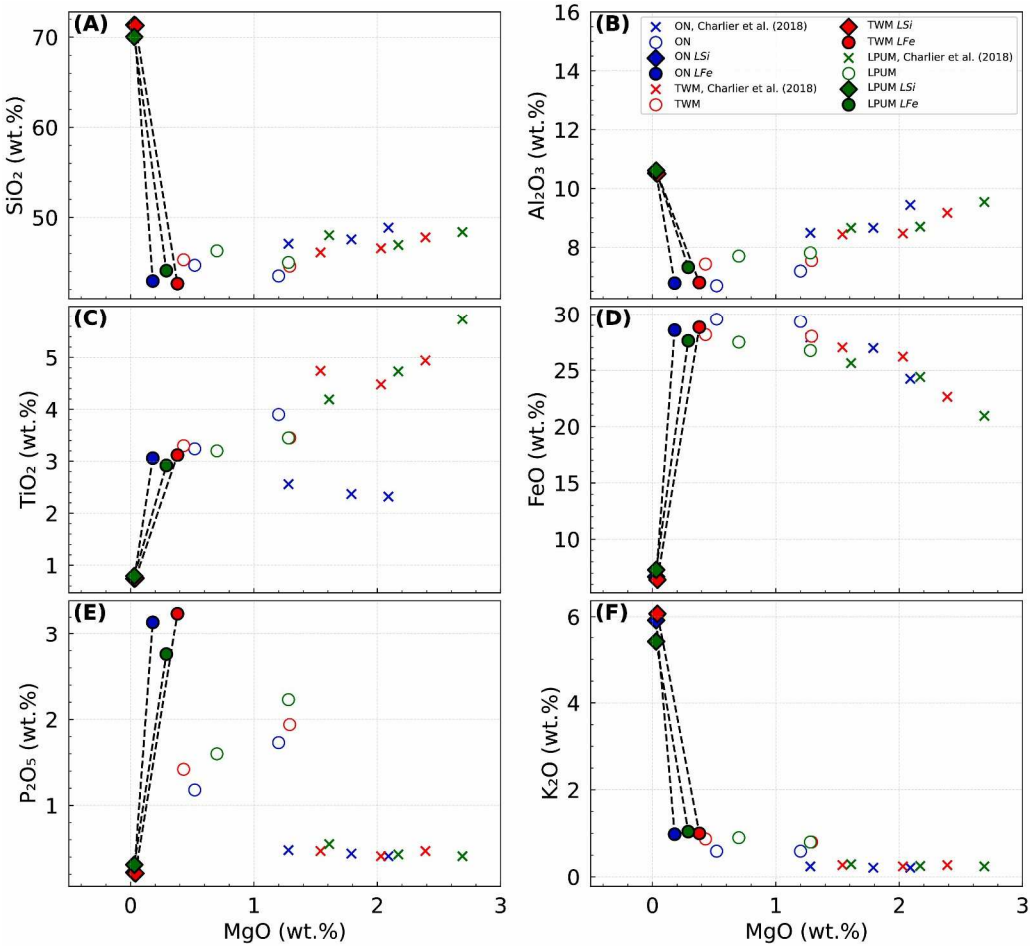

Fig. 4. Selected major elemental concentrations in the melt as a function of melt MgO content. Dashed lines connect immiscible melt pairs. Symbols are identical to Fig. 3.

Eqs. (2–4) are dependent on mineral and melt densities. Mineral densities were calculated using a third-order Birch-Murnaghan equation of state (EOS, Supplementary Material). For the melt density, we apply a modified version of the EOS of silicate presented by Lange and Carmichael (1990) and Kress and Carmichael (1991) that is self-consistent with the interior structure of the Moon (see Supplementary Material). The temperature profile is calculated from the adiabatic temperature gradient with dT/dP = ‗ 44 K/GPa (Kraettli et al., 2022). The surface temperature is calculated from the liquid thermometer in Charlier et al. (2018), which ranged from 1470 ˚C to 1540 ˚C depending on the bulk Moon composition considered (Supplementary Material). To solve the LMO model, we integrate Eqs. (2, 3) with the EOSs and set the following conditions as initial boundary conditions:

$$P(R_0) = 0 \tag{5}$$

$$g(R_0) = \frac{GM(R)}{R_0^2} \tag{6}$$

Published in : Earth and Planetary Science Letters (2024), vol. 646, 118989
DOI: 10.1016/j.epsl.2024.118989
Status : Postprint (Author's version)

where R_0 and $M(R)$ are the present-day average radius (1737 km) and mass (7.342×10^{22} kg) of the Moon. The boundary conditions of the LMO are modified when plagioclase floats to form the crust:

$$R_b = R_0 - d \tag{7}$$

$$P(R_b) = \int_{R_b}^{R} g(x)\rho_{pl}dx \tag{8}$$

$$g(R_b) = \frac{GM_{R_b}}{R_b^2} \tag{9}$$

where d is crustal thickness, ρ_{pl} is the density of plagioclase, R_b is the radius at the base of the crust, and M_{R_b} is the residual mass of the LMO below R_b.

Using this model, we map a bottom-up LMO differentiation sequence by combining the experimentally determined mineral crystallization sequence and cotectic proportions (Supplementary Materials). Because our model allows us to account for plagioclase accumulation at the bottom or flotation at the top of the LMO, we also calculate the theoretical thickness of the anorthosite crust as a function of flotation efficiency. For self-consistency, we consider a shallow LMO endmember (bottom pressure ~2.8 GPa at 600 km depth) as adopted by Charlier et al. (2018). For comparison, however, we also upscaled the outputs of the shallow models to a whole-Moon magma ocean (Supplementary Material).

3. Results

3.1. PHASE EQUILIBRIA AND IMMISCIBLE TEXTURES

The silicate liquids produced in our experiments are multiply saturated with plagioclase, augite, silica (tridymite or β-quartz) and ilmenite (± fayalitic olivine ± pigeonite; Figs. 2 and S1). Olivine, augite, plagioclase, and ilmenite are stable in all experiments, except one of LPUM composition at 1020 °C that lacks olivine. Silica is stable in all studied compositions, as reported in other experimental studies (Lin et al., 2017a; Charlier et al., 2018; Rapp and Draper, 2018); indeed, silica is present at 1080 °C and below in the experiments of Charlier et al. (2018). Our results are also consistent with higher-temperature data indicating the instability of olivine at 1220–1020 °C (Charlier et al., 2018); olivine is present above and below this temperature gap, which is due to the destabilization of low-Ca pyroxene. Ilmenite saturation primarily depends on the starting composition and its TiO_2 content; ilmentite appears between 1060 and 1020 °C in the experiments of Charlier et al. (2018), and is therefore present in all present experiments.

Published in : Earth and Planetary Science Letters (2024), vol. 646, 118989
DOI: 10.1016/j.epsl.2024.118989
Status : Postprint (Author's version)

A two-liquid field is reached for all compositions at 1000 °C and 0.8 GPa. Micrometer-sized globules of Si-rich melt develop within the Ferich melt with sharp two-liquid interfaces (Fig. 2B). Si-rich melt droplets wet plagioclase with high wetting angles, are often entrapped in fayalitic olivine, and form irregular melt pools. These textures are similar to those observed in previous experiments on Fe-rich lunar basalts in which immiscibility developed (e.g., Rutherford et al., 1974).

3.2. COMPOSITION OF THE EXPERIMENTAL LIQUIDS

Electron microprobe analyses of experimental liquids and solid phases are reported in Supplementary Dataset Table S1. The compositions of our late-stage residual melts are plotted with those obtained at higher temperatures up to 1080 °C by Charlier et al. (2018) against experimental temperature in Fig. 3 and against melt MgO (Fig. 4) and SiO_2 contents (Fig. S2). Late-stage residual melts show Al_2O_3, and MgO, depletion, and extreme iron enrichment up to 28–29 wt.% FeO. TiO_2 contents increase continuously until ilmenite saturation, then decrease markedly. Similar trends have been reported by other studies on LMO differentiation (Lin et al., 2017a, 2017b; Rapp and Draper, 2018).

Our experiments show that the liquid line of descent reaches a binodal surface at 1000 °C, resulting in the separation of two immiscible melts: a Si-rich rhyolitic melt and a Fe-rich ferrobasaltic melt. All three bulk compositions produce similar immiscible melt compositions. The Si-rich melts (70.0–71.4 wt.% SiO_2, 6.4–7.3 wt.% FeO) are enriched in Al_2O_3 (10.5–10.6 wt.%), Na_2O (0.7–1.0 wt.%), and K_2O (5.4–6.1 wt.%) but depleted in TiO_2 (0.7–0.8 wt.%) and P_2O_5 (0.2–0.3 wt.%). They also have low CaO/Al_2O_3 ratios (~0.28). In contrast, the Fe-rich melts (42.6–44.1 wt.% SiO_2, 27.6–28.8 wt.% FeO) are depleted in Al_2O_3 (6.8–7.3 wt.%), Na_2O (0.2–0.4 wt.%) and K_2O (0.9–1.0 wt.%) but enriched in TiO_2 (2.9–3.1 wt.%) and P_2O_5 (2.8–3.2 wt.%) and have higher CaO/Al_2O_3 ratios (~1.67). Both immiscible melts are extremely depleted in MgO (<1 wt.%). The contrasting compositions lead to distinct physical properties, with the Si-rich melts being less dense (on average, ρ = 2441 kg/m^3, calculated from the EOS; Section 2.5, Supplementary Material) but more viscous (755.3 Pa s, calculated after Hui and Zhang, 2007), than the dense (ρ =3040 kg/m^3), low-viscosity (88.5 Pa s) Fe-rich melts. Partitioning coefficients between the Fe-rich and Si-rich melts ($D_{LFe/LSi}$) are reported in Table 3. The compositions of the immiscible pairs observed in this study and their liquid–liquid partitioning coefficients are similar to those produced experimentally during the last stage of evolution of mare basalts (Longhi 1990; Rutherford et al., 1974; Hess et al., 1975, 1978).

Published in : Earth and Planetary Science Letters (2024), vol. 646, 118989
DOI: 10.1016/j.epsl.2024.118989
Status : Postprint (Author's version)

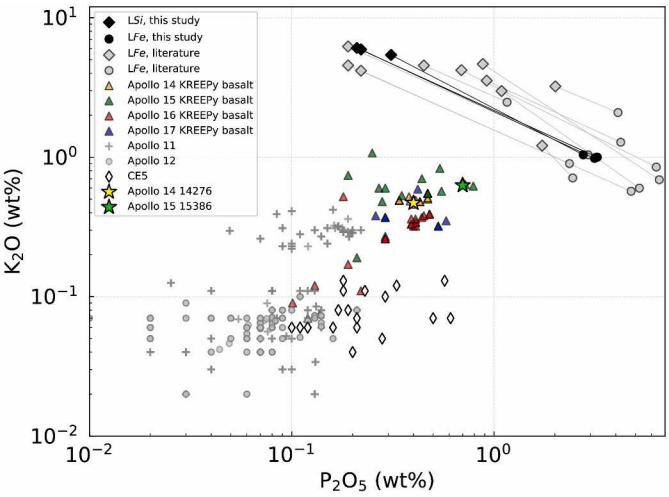

Fig. 5. K_2O and P_2O_5 concentrations of experimental immiscible melts compared to those of Apollo lunar rocks. KREEPy basalts are shown in color: Apollo 14–17 basalts (triangles), including Apollo 14 14,276 and Apollo 15 15,386 as representative KREEPy basalts. Non-KREEPy basalts: Apollo 11 and 12 basalts and Chang'E 5 (CE5) ferrobasalts. Literature immiscibility experiments are from Longhi (1990), Roedder and Weiblen (1970), Rutherford et al. (1974), Hess et al. (1975), and Gullikson et al. (2016). Solid lines connect immiscible melt pairs.

4. Discussion

4.1. ILMENITE CRYSTALLIZATION AND THE FORMATION OF EVOLVED HIGH-TI CUMULATES

The crystallization of ilmenite during the late-stage evolution of the LMO was a major event during lunar history. Ilmenite is the principal Tibearing mineral responsible for the formation of dense cumulates that might have triggered gravitational instability and overturn of the cumulate pile (Herbert, 1980; Hess and Parmentier, 1995; Elkins-Tanton et al., 2002; Prissel et al., 2024), in turn forming the source of high-Ti basalts (Longhi et al., 1974; Krawczynski and Grove, 2012). It was also suggested that an ilmenite-rich layer could be an important component of the core (Parmentier et al., 2002; de Vries et al., 2010). However, the degree of melt evolution at ilmenite saturation (thus the thickness of the ilmenite-bearing layer) and the abundance of ilmenite in the cumulate (thus the density of the ilmenite-rich layer) remain poorly constrained.

Ilmenite was previously considered to appear very late (>95 PCS) in the model of Snyder et al. (1992), but much earlier (87 PCS) by Elkins-Tanton et al. (2011). Indeed, the stability of ilmenite is composition and temperature dependent (Charlier et al., 2018; Zhang et al., 2023), as evidenced by ilmenite saturation at 95–97 PCS in a variety of bulk LMO compositions (0.17–0.31 wt.% TiO_2) in those studies. Other recent experiments with relatively high TiO_2 concentrations in the bulk lunar composition (0.5 wt.%) saturates ilmenite at ~91 PCS (Lin et al., 2017b), and earlier in hydrous melts (~88 PCS; Lin et al., 2017a). In our experiments and those of Charlier et al. (2018), ilmenite saturates at different PCS in the three investigated compositions, coexisting with plagioclase, pigeonite, augite, and

Published in : Earth and Planetary Science Letters (2024), vol. 646, 118989
DOI: 10.1016/j.epsl.2024.118989
Status : Postprint (Author's version)

a silica phase. The high-density pyroxene phase pigeonite may be present in ilmenite-bearing cumulates or replaced at lower temperature (<1020 °C) by fayalitic olivine.

In our LMO model (Section 2.5), ilmenite saturation is affected by the trapped liquid fraction within the cumulate pile. This is because the trapped liquid fraction affects the bulk partition coefficients of incompatible elements like Ti (Fig. S3), even at the low fractions (<5%) modeled for magma oceans and intrusions on Earth (Solomatov, 2007; McKenzie, 2011). Our LMO model of a low-TiO_2 LPUM composition shows that ilmenite appears at ~97 PCS in the absence of trapped liquid and at 98 PCS for 10% trapped liquid. Assuming the radius of the present-day Moon and 60% plagioclase flotation efficiency (the percentage of plagioclase that floats to form crust vs. that which accumulates at the bottom of the LMO), our model indicates ilmenite saturation at 6.6 km depth in the absence of trapped liquid and shallower ilmenite saturation at 3.3 km depth for 10% trapped liquid. Under more efficient plagioclase flotation (80%), these respective ilmenite saturation depths decrease to 2.8 and 2.9 km.

When ilmenite joins the crystallization assemblage, the density of the mantle increases from ~3150–3300 kg/m^3 for an ilmenite-free mantle to ~3550–3890 kg/m^3 for an ilmenite-bearing mantle (ranges reported for plagioclase floatation efficiencies of 60–100%, respetively). This density increasing causes gravitational instability in the mantle, though we note that fractional crystallization of silicates will also produce an earlier gravitational instability as the Mg# evolves (e.g., Hess and Parmentier, 1995). Indeed, gravitationally induced mantle overturn has been invoked to explain the KREEP enrichment in the lunar mantle source (Zhang et al., 2022), which requires ilmenite to be associated with the urKREEP reservoir or KREEP-rich component. However, many models have concluded that the high levels of KREEP enrichment observed in high-K KREEPy basalts (Warren et al., 1987) and the hypothetical urKREEP component (Warren and Wasson, 1979) require >99 PCS (e.g., Snyder et al., 1992; Jing et al., 2022), whereas our experiments and models, as well as previously published experiments, show that ilmenite crystallized earlier. We note that low degree melting of the mantle source may also produce melt enriched in KREEP component. Therefore, the segregation of ilmenite alone may not necessarily enrich mantle sources in the KREEP signature as much as the enrichment expected in late-stage LMO residual liquids. We note that recent LMO experiments also crystallized high-density Ti-spinel as a major oxide phase late during differentiation (Schmidt and Kraettli, 2022), although this can be attributed to the relatively high fO_2 (ΔIW +1.1) in their experiments, which favors the stabilization of spinel.

4.2. ONSET OF IMMISCIBILITY IN THE LMO

The occurrence of immiscibility between Fe-rich and Si-rich melts in lunar rocks was first observed in melt inclusions in Apollo samples (Roedder and Weiblen, 1970). Subsequent experiments to constrain the liquid lines of descent of mare basalts identified that immiscibility occurred very late during crystallization (Rutherford et al., 1974; Hess et al., 1975, 1978). It was then inferred that the residual products of the LMO would also have reached liquid immiscibility after the formation of the anorthositic crust (Longhi, 1990; Hess et al., 1975), although the scale of melt separation was unknown (Taylor et al., 1980; Neal and Taylor, 1989).

Published in : Earth and Planetary Science Letters (2024), vol. 646, 118989
DOI: 10.1016/j.epsl.2024.118989
Status : Postprint (Author's version)

In our experiments, we demonstrated that immiscibility develops late during LMO differentiation, under conditions similar to those observed in experiments on lunar mare basalts, namely <1050 °C (Longhi 1990; Rutherford et al., 1974; Hess et al., 1975, 1978). The Si-rich and Fe-rich melts produced herein are compositionally similar to immiscible melts obtained in those experiments (Fig. 5), particularly the preferential partitioning of K into Si-rich melt ($D_{LFe/LSi}$ = 0.17 ± 0.01) and P into the Fe-rich melt ($D_{LFe/LSi}$ = 12.87 ± 2.84; Table 3).

Thermodynamically, immiscibility arises when the total Gibbs free energy of the immiscible phases is lower than that of a single liquid phase at given pressure and temperature conditions (Ghiorso and Carmichael, 1980). However, the thermodynamic complexity of multi-component silicate liquids precludes accurate prediction of the onset of immiscibility in lunar residual melts. Nonetheless, Zhang et al. (2023) used the composition of published experimental unmixed pairs (lunar and other compositions) to define an empirical solvus. Accordingly, any liquid line of descent undergoes unmixing if it intersects or plots below the solvus (see Fig. 6):

$$RT\ln X_{SiO_2} = \frac{4.6 \times 10^{-4} \times \left((-14736.5 - \phi)^2 - 12323.9 \times (\phi^2)\right)}{2.155} \quad (10)$$

where X_{SiO_2} is the mole percentage of SiO_2 in the liquid and ϕ is the sum of the mole percentages of oxides dominantly partitioning into the Ferich melt, i.e. $X_{TiO_2} + X_{FeO} + X_{MgO} + X_{CaO} + X_{P_2O_5}$. In this model, the left side of the equation reflects the compositional evolution of liquid lines of descent and the right side represents the compositional dependence of the solvus. We tested the validity of this expression with our experimental results presented herein and obtained a coefficient of determination on the test dataset (r_{test}^2) of 0.99, with a root mean square error (RMSE) of 146, which is 78% smaller than the standard error estimation of the original fit. This validates the application of the predictive immiscibility model to our LMO differentiation path (Fig. 6).

Fig. 7 shows the results of our LMO model incorporating the influence of plagioclase flotation efficiency on the anorthositic crustal thickness and the influence of the trapped liquid fraction on the evolution of the liquid lines of descent. Previous studies showed that plagioclase flotation efficiency of 60–80% might reproduce the lunar crustal thickness (average 49 ± 16 km;) measured by the Gravity Recovery and Interior Laboratory mission (Wieczorek et al., 2013; Charlier et al., 2018); reduced plagioclase flotation efficiency would produce a thinner crust from an entire magma ocean. An increased fraction of trapped liquid slows fractionation (Fig. S3). Importantly, immiscibility could not develop if the trapped liquid fraction much exceeded 10% because the liquid line of descent would not intersect the solvus. In our results, immiscibility occurs at 97–98 PCS (Fig. 7). The depth at which immiscibility develops during LMO differentiation correlates with the degree of plagioclase flotation (i.e. the thickness of anorthositic crust), ranging from ~40 km depth for 60% plagioclase flotation to ~50 km for 80% plagioclase flotation (Fig. 7). The trapped liquid fraction also impacts the depth range over which immiscibility could develop, which ranges from 6.7 to 3.1 km thick for 0 to 10% trapped liquid, respectively, at 60% plagioclase flotation, and from 2.9 to 2.7 km thick for 0 to 10% trapped liquid, respectively, at 80% plagioclase flotation. Based on the average relative proportions of immiscible melts observed in our experiments (Fe-rich melt/Si-rich melt ratio of ~10; Table 2), if the two melts with distinct densities and viscosities could fully segregate, the Si-rich and Fe-rich layers

Published in : Earth and Planetary Science Letters (2024), vol. 646, 118989
DOI: 10.1016/j.epsl.2024.118989
Status : Postprint (Author's version)

would be ~0.4 and ~4.3 km thick, respectively, at 60% plagioclase flotation or 0.3 and 2.5 km thick, respectively, at 80% plagioclase flotation.

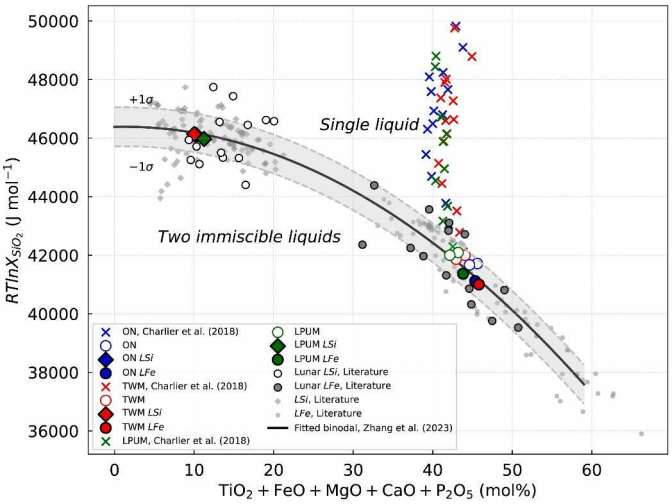

Fig. 6. Testing the immiscibility prediction of Zhang et al. (2023) for immiscibility experiments in this study. The r_{test}^2 value for our new experimental dataset is 0.99. Lunar literature data are lunar immiscibility experiments from Rutherford et al. (1974), Hess et al. (1975, 1978), Longhi (1990), and Gullikson et al. (2016). Other literature data are non-lunar immiscibility experiments from Ryerson and Hess (1978, 1980), Dixon and Rutherford (1979), Charlier and Grove (2012), Hou et al. (2017, 2018), Honour et al. (2019) and Zhang et al. (2023).

4.3. IMMISCIBLE URKREEP, THE ORIGIN OF THE KREEP COMPONENT, AND IMPLICATIONS FOR LUNAR SILICIC MAGMATISM

The KREEP component has significantly influenced the evolution of lunar rocks by facilitating the remelting of the mantle lithologies. This was mainly caused by melting-point depression as a result of hybridization with evolved lithologies and by the preservation of heat producing elements in the KREEP component (Dowty et al., 1976; Elardo et al., 2020). The presence of the KREEP component in primitive lithologies also provides valuable information about the lunar interior and its early evolution, and supports the formation of highly evolved lithologies in the LMO model (Warren and Wasson, 1979; Warren, 1985). Furthermore, many Apollo samples contain a KREEP component. However, the origin of lunar materials with a significant KREEP component remains highly debated, with two main hypotheses being argued: (1) an impact mixed the urKREEP or KREEP component with more primitive lithologies (Ryder and Bower, 1976; McKay et al., 1978); or (2) primitive melts or mantle sources assimilated urKREEP, followed by fractionation or partial melting of a KREEP-rich interior (Dowty et al., 1976; Irving, 1977; Ryder, 1987), possibly induced by a cumulate overturn event (Ringwood and Kesson, 1976). KREEPy rocks formed via the impact process have been identified in Apollo 14 samples from Fra Mauro and Apollo 16 samples from the Descartes highlands (McKay et al., 1978). In contrast, porphyritic textural evidence in Apollo 15 and Apollo 17 rocks was interpreted as having formed by

Published in : Earth and Planetary Science Letters (2024), vol. 646, 118989
DOI: 10.1016/j.epsl.2024.118989
Status : Postprint (Author's version)

partial melting of a KREEP-rich interior (Ryder, 1988), although recent studies suggest that the identified phenocrysts may have originated from an unrelated magma (e.g., Cronberger and Neal, 2017).

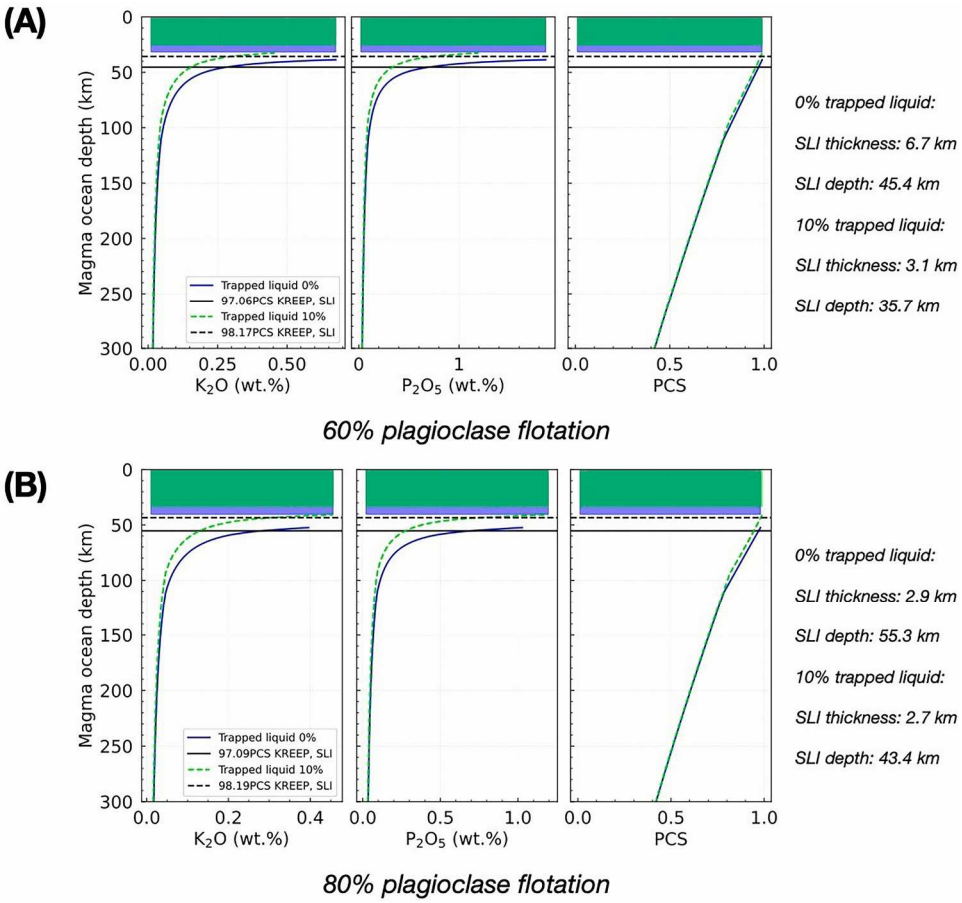

Fig. 7. Forward modeling of the LMO for the LPUM composition (Longhi, 2006) with a shallow magma ocean (~600 km deep, the figure is scaled to 300 km). Modeling results for (A) 60% and (B) 80% plagioclase flotation efficiency during LMO differentiation. Both figures show the evolution of K_2O and P_2O_5 concentrations and percent solidification in the cumulate column. The dashed and solid horizontal lines show the onset of silicate liquid immiscibility with 0% and 10% liquid trapped in the cumulate, respectively. Green and blue areas represent the modelled thickness of the anorthositic crust with 10% trapped liquid and 0% trapped liquid, respectively.

Published in : Earth and Planetary Science Letters (2024), vol. 646, 118989
DOI: 10.1016/j.epsl.2024.118989
Status : Postprint (Author's version)

Table 2
Experimental conditions and phase assemblages and proportions.

Start. Comp.[a]	Run no.	*P* (GPa)	*T* (°C)	Duration (h)	Capsule	Phases[c]	Σr^2	*LFe /LSi*[d]
ON/02–3[a]	HA11–1	0.1	1020	148	C + Pt	gl (3), ol (1), aug (55), plag (31), sil (7), ilm (2)	0.28	–
ON/04–1.5	HA10–1	0.10	1010	148	C + Pt	gl (29), ol (15), aug (24), plag (20), sil (9), ilm (2)	0.23	–
ON/04–1.5	HA03–0.8	0.08	1000	138	C + Pt	Si-gl (11), Fe-gl (1), ol (20), aug (30), plag (24), sil (11), ilm (3)	0.46	10.4
ON/04–1.5	HA12–1[b]	0.10	980	140	C + Pt	Si-gl, Fe-gl, ol, aug, plag, sil, ilm		
TWM/02–3[a]	HA11–1	0.1	1020	148	C + Pt	gl (0), ol (3), aug (55), plag (32), sil (6), ilm (5)	0.46	–
TWM/04–1.5	HA10–1	0.10	1010	148	C + Pt	gl (20), ol (12), aug (31), plag (21), sil (9), ilm (7)	0.33	–
TWM/04–1.5	HA03–0.8	0.08	1000	138	C + Pt	Si-gl (9), Fe-gl (2), ol (15), aug (32), plag (24), sil (10), ilm (8)	0.63	6.9
TWM/04–1.5	HA12–1[b]	0.10	980	140	C + Pt	Si-gl, Fe-gl, ol, aug, plag, sil, ilm		
LPUM/02–3[a]	HA11–1	0.1	1020	148	C + Pt	gl (0), aug (53), plag (34), sil (6), ilm (7)	0.56	–
LPUM/04–1.5	HA10–1	0.10	1010	148	C + Pt	gl (25), ol (10), aug 27), plag (22), sil (9), ilm (6)	0.28	–
LPUM/04–1.5	HA03–0.8	0.08	1000	138	C + Pt	Si-gl (11), Fe-gl (2), ol (13), aug (33), plag (25), sil (10), ilm (6)	0.62	12.6
LPUM/04–1.5	HA12–1[b]	0.10	980	140	C + Pt	Si-gl, Fe-gl, ol, aug, plag, sil, ilm		

[a] Starting materials are from Charlier et al. (2018).
[b] Near-solidus experiments; phases were not analyzed, only BSE images were acquired.
[c] Phase proportions estimated from the compositional matrix by using a non-negative least squares regression algorithm (Zhang et al., 2023).
[d] The ratio of immiscible melt pairs estimated by mass balance of the K_2O and P_2O_5 contents of the immiscible pairs with those of the bulk compositions.

Table 3
Immiscible melt compositions.

Start. Comp.	*P* (GPa)	*T* (°C)	Run No.		SiO_2	TiO_2	Al_2O_3	FeO	MnO	MgO	CaO	Na_2O	K_2O	P_2O_5	Total
ON/04–1.5	0.08	1000	HA03–0.8	*LFe*[a]	42.95	3.06	6.78	28.57	0.45	0.18	11.42	0.33	0.98	3.14	97.87
				LSi	71.35	0.74	10.52	6.68	0.11	0.03	2.92	0.75	5.92	0.22	99.24
				$D_{LFe/LSi}$[b]	0.60	4.14	0.64	4.28	4.09	6.00	3.91	0.44	0.17	14.27	
TWM/04–1.5	0.08	1000	HA03–0.8	*LFe*	42.66	3.12	6.80	28.83	0.60	0.38	11.40	0.25	1.00	3.24	98.29
				LSi	71.28	0.75	10.50	6.41	0.11	0.04	2.85	0.65	6.07	0.21	98.86
				$D_{LFe/LSi}$	0.60	4.16	0.65	4.50	5.45	9.50	4.00	0.38	0.16	15.43	
LPUM/04–1.5	0.08	1000	HA03–0.8	*LFe*	44.10	2.92	7.32	27.62	0.30	0.29	11.10	0.43	1.04	2.76	97.88
				LSi	70.03	0.79	10.61	7.29	0.06	0.03	3.15	1.01	5.41	0.31	98.65
				$D_{LFe/LSi}$	0.63	3.70	0.69	3.79	5.00	9.67	3.52	0.43	0.19	8.90	

[a] *LFe* and *LSi* are the Fe-rich and Si-rich melts, respectively.
[b] $D_{LFe/LSi}$ are partition coefficients between the Fe-rich and Si-rich melts.

Both hypotheses require a post-LMO hybridization event involving very late-stage urKREEP melts (Warren and Wasson, 1979; Snyder et al., 1992). In our experiments and models, we show that immiscibility develops at the very late stage of LMO differentiation (Figs. 7 and S4). Therefore, the liquid may have split into a K-Si-rich fraction and a REEP-Fe rich fraction. Given the density and viscosity contrasts between the two fractions, it can be expected that these immiscible pairs might have become segregated and unevenly distributed. Therefore, the contamination of KREEP-poor primitive melts by these immiscible endmembers might produce the *K* + REEP-enriched signature observed in KREEPy rocks (Figs. 1 and 5). Such contamination could have occurred through various magmatic processes including assimilation during magma ascent or the direct incorporation of the urKREEP or KREEP component in the mantle source. In addition, Dowty et al. (1976) proposed that urKREEP might remain molten or be easily remelted due to its high concentration of heat-producing elements. The intense meteorite bombardment that formed the Imbrium basin might therefore have exposed the urKREEP melts, forming the large PKT (e.g., Jolliff et al., 2000). It is thus plausible that melts derived from the partial melting of REEP-Fe-rich and K-Si-rich lithologies became enriched in *K* + REEP, eventually contributing to the KREEP component.

To conclude our discussion, we use assimilation as a simple example to demonstrate how immiscible urKREEP melt can result in KREEP enrichment in lunar rocks and estimate the likely proportion of immiscible urKREEP. We stress that assimilation is not the only mechanism that can contribute to KREEP enrichment. For instance, the melting of a hybridized cumulate with a small KREEP enrichment can reproduce the high KREEP signature in Mg-suite troctolites (Hess, 2000). Our aim here is to convincingly demonstrate that the incorporation of immiscible urKREEP melt can, to some extent,

Published in : Earth and Planetary Science Letters (2024), vol. 646, 118989
DOI: 10.1016/j.epsl.2024.118989
Status : Postprint (Author's version)

explain the KREEP signature in lunar rocks. More work would of course be necessary to detail the actual contribution of immiscible urKREEP melt to natural lunar rocks.

For this demonstration, we present a mixing model to quantify the likely fractions of immiscible urKREEP in lunar rocks, considering two assimilation scenarios: (1) the direct assimilation of immiscible urKREEP melts and (2) the assimilation of melts produced by the partial melting of the crystallization products (cumulates) of the immiscible KSi-rich and REEP-Fe rich lithologies. We use mass balance to calculate the mixing of the KREEP-free component, the K-Si-rich component, and the REEP-Fe component. Compared to KREEP-free rocks, KREEPy rocks typically exhibit major element enrichments of K and P and have lower Ca/Al ratios (Fig. 1). KREEPy rocks also have variable Mg# and FeO and SiO_2 contents. These characteristics imply that prior to KREEP assimilation, the primitive magma likely experienced varying degrees of differentiation or derived from a range of mantle sources, leading to broadly variable MgO, FeO, and SiO_2 contents. The K and P concentrations in an evolved magma are significantly low (<1 wt.%) before undergoing processes like silicate liquid immiscibility or extreme fractional crystallization (≳4 wt.%). Hence, we can leverage K, P, and Ca/Al to estimate the likely maximum proportions of assimilated immiscible urKREEP, i.e. its K-Si-rich and P-Fe rich fractions. We did not include REEs in our mixing model, but because they are expected to partition into the Fe-rich melts, we used P as a proxy for REEs. As an estimate of KREEP-free K and P concentrations and CaO/Al_2O_3, we take the compositions of Apollo 11 and Apollo 12 basalts (median values of 0.07 wt.% K_2O, 0.08 wt.% P_2O_5, and CaO/Al_2O_3 = 1.09) as representative of non-KREEPy rocks. The composition of immiscible urKREEP is calculated by averaging the immiscible melt compositions from our experiments. Regarding the partial melting of the Si-rich and Fe-rich lithologies in scenario (2), we assume K and P to be fully incompatible during the melting of both lithologies; therefore, K and P concentrations can be used as an approximation of the degree of melting of both lithologies, and thus of as their contribution to the formation of the KREEP component.

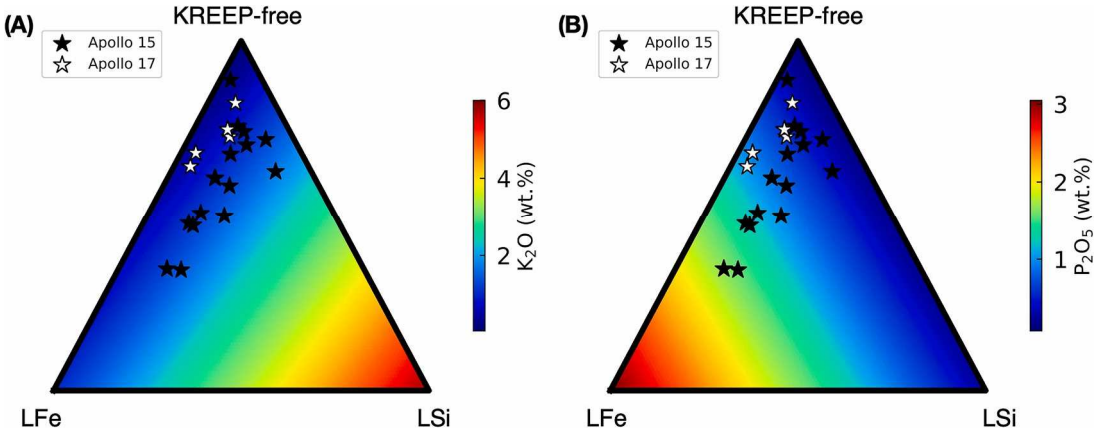

Fig. 8. Modelled K_2O and P_2O_5 compositions in a KREEP-free melt mixed with immiscible urKREEP Fe-rich (LFe) and Si-rich melts (LSi). The KREEP-free melt is based on median values of non-KREEPy Apollo 11 and Apollo 12 basalts (see Section 4.3). Stars show mass balance estimates of the proportions of immiscible urKREEP melts assimilated to form the KREEP components in the Apollo 15 and Apollo 17 rocks.

Published in : Earth and Planetary Science Letters (2024), vol. 646, 118989
DOI: 10.1016/j.epsl.2024.118989
Status : Postprint (Author's version)

We focus our calculations on Apollo 15 and Apollo 17 rocks because they are the most likely to have originated from the melting of a KREEPbearing mantle source (Neal et al., 2015; Cronberger and Neal, 2019). Fig. 8 shows the result for K_2O and P_2O_5 in scenario (1). The calculations show that the formation of the KREEP component in Apollo 15 basalts requires the assimilation of 8–52% Fe-rich melt and 3–28% Si-rich melt. Similarly, the formation of the KREEP component in Apollo 17 basalts requires 10–31% Fe-rich melt and 4–11% Si-rich melt. We show that it is thermodynamically possible to assimilate this much cold liquid in the Supplementary Material. The noticeably higher proportion of Fe-rich melt assimilation is attributed to the dominance of Fe-rich melts during LMO differentiation, consistent with our experimental observations that relatively low proportions of Si-rich droplets coexist within more abundant Fe-rich melts (Table 2). Additionally, the higher viscosity of Si-rich melts may also hinder their pooling to form larger, assimilable volumes. Fig. 9 shows the results of the degree of partial melting of the Fe-rich and Si-rich lithologies required in scenario (2). As in scenario (1), forming the KREEP component in Apollo 15 and Apollo 17 basalts requires a higher degree of partial melting of the Fe-rich lithology (median = 60%) and less melting of the Si-rich lithology (median = 40%).

Additionally, lunar samples contain evolved rocks such as granites and felsites (Warren et al., 1983, 1987; Jolliff, 1991), and granite plutons have been identified on the lunar surface, such as the Gruithuisen Domes (Chevrel et al., 1999) and the Compton–Belkovich Thorium Anomaly (Jolliff et al., 2011). Silicate liquid immiscibility is often considered to play a crucial role in the formation of evolved lunar rocks (e.g., Jin et al., 2024) because lunar granites have significantly high K/REE and K/P ratios (e.g., Warren et al., 1983), which can be explained by the segregation of a Si-rich immiscible melt. However, Apollo-returned granites have high U/REE and Th/REE ratios (Warren et al., 1983, 1987), which seem to contradict the expected composition of a segregated Si-rich immiscible melt because U and Th should preferentially partition into the Fe-rich melt (Veksler et al., 2006). Nonetheless, this cannot preclude the contribution of immiscibility because the trace elemental ratios in the immiscible melts depend on the ratios in their parental melt. Some researchers have proposed crustal remelting to explain the compositions of the granites (e.g., Gullikson et al. 2016), which could also account for large-scale silicic magmatism. However, our experiments and models demonstrate that during the late stages of LMO differentiation, silicate liquid immiscibility could have developed, and produced K-Si-rich melts capable of forming K-Si-rich but REE-poor lithologies. Furthermore, the partial melting of such lithologies or the extraction of Si-rich melts will tend to produce melts with high K/REE and K/P ratios. Therefore, we speculate that the Si-rich immiscible melt that formed late during LMO differentiation may have contributed to the formation of lunar granites. Further work is needed to better understand the contribution of this LMO-derived Si-rich lithology to evolved lunar rocks.

Published in : Earth and Planetary Science Letters (2024), vol. 646, 118989
DOI: 10.1016/j.epsl.2024.118989
Status : Postprint (Author's version)

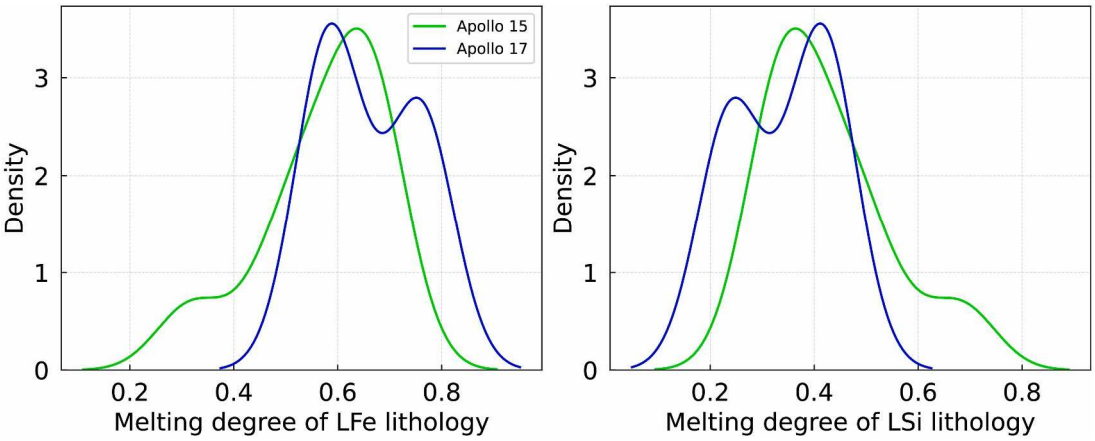

Fig. 9. Estimated degrees of melting of the Fe-rich (LFe) and Si-rich lithologies (LSi) required to form the KREEP components in the Apollo 15 and Apollo 17 rocks.

5. Conclusions

We experimentally investigate the very late stage differentiation of the LMO, aiming to test the hypothesis that urKREEP could be produced by silicate liquid immiscibility. Using three silicate melt compositions representative of the LMO, we produced immiscibile K-Si-rich and P-Ferich melts in all compositions at 1000 ˚C and <97% crystallization. We also used a LMO model to investigate the conditions and depths of the onsets of ilmenite crystallization and immiscibility. The development of immiscibility can form immiscible urKREEP melts earlier than in the case of extreme fractional crystallization. We also discussed the possibility of forming KREEPy rocks by the contamination of primitive melts with immiscible urKREEP melts, considering processes such as both the direct assimilation of immiscible melts and assimilation of melts derived from the partial melting of Fe-rich and Si-rich lithologies. We demonstrate the potential role of silicate liquid immiscibility in hybridization. Finally, the K-Si-rich immiscible lithology may have contributed to lunar silicic magmatism.

CRediT authorship contribution statement

Yishen Zhang: Writing – original draft, Visualization, Methodology, Investigation, Data curation. **Bernard Charlier:** Writing – review & editing, Writing – original draft, Investigation, Funding acquisition, Formal analysis, Conceptualization. **Stephanie B. Krein:** Writing – review & editing, Investigation. **Timothy L. Grove:** Writing – review & editing, Resources, Methodology, Funding acquisition, Conceptualization. **Olivier Namur:** Writing – review & editing, Methodology, Investigation, Funding acquisition. **Francois Holtz:** Writing – review & editing, Resources, Methodology, Funding acquisition.

Published in : Earth and Planetary Science Letters (2024), vol. 646, 118989
DOI: 10.1016/j.epsl.2024.118989
Status : Postprint (Author's version)

Declaration of competing interest

The authors declare that they have no known competing financial interests or personal relationships that could have appeared to influence the work reported in this paper.

Data availability

Data has been attached along with the submission.

Acknowledgements

BC acknowledges support by a Marie Curie International Outgoing Fellowship within the 7th European Community Framework Programme. This work was supported by the Fonds de la Recherche Scientifique – FNRS under Grant 33653710. BC is a Research Associate of the Belgian Fund for Scientific Research-FNRS. Discussions with Oliver Shorttle, Attilio Rivoldini, and Dian Ji are highly appreciated. R. Dennen is thanked for his help in editing the manuscript. We thank Frederic Moynier for editorial handling. Constructive comments from Nick Dygert and an anonymous reviewer significantly improved the quality of the paper.

Supplementary materials

Supplementary material associated with this article can be found, in the online version, at doi:10.1016/j.epsl.2024.118989.

References

Barnes, J.J., Tartese, R., Anand, M., McCubbin, F.M., Neal, C.R., Franchi, I.A., 2016. Early degassing of lunar urKREEP by crust-breaching impact (s). Earth Planet. Sci. Lett. 447, 84–94.

Benne, D., Behrens, H., 2003. Water solubility in haplobasaltic melts. Eur. J. Mineral. 15, 803–814.

Berndt, J., Liebske, C., Holtz, F., Freise, M., Nowak, M., Ziegenbein, D., Hurkuck, W., Koepke, J., 2002. A combined rapid-quench and H2-membrane setup for internally heated pressure vessels: description and application for water solubility in basaltic melts. Am. Mineralog. 87, 1717–1726.

Cameron, A.G., Ward, W.R., 1976. The origin of the Moon. In: Abstracts of the Lunar and Planetary Science Conference, 7, p. 120. Page(1976).

Canup, R.M., 2012. Forming a Moon with an Earth-like composition via a giant impact. Science (1979) 338, 1052–1055.

Charlier, B., Grove, T.L., 2012. Experiments on liquid immiscibility along tholeiitic liquid lines of descent. Contrib. Mineral Petrol. 164, 27–44. https://doi.org/10.1007/ s00410-012-0723-y.

Published in : Earth and Planetary Science Letters (2024), vol. 646, 118989
DOI: 10.1016/j.epsl.2024.118989
Status : Postprint (Author's version)

Charlier, B., Grove, T.L., Namur, O., Holtz, F., 2018. Crystallization of the lunar magma ocean and the primordial mantle-crust differentiation of the Moon. Geochim. Cosmochim. Acta 234, 50–69. https://doi.org/10.1016/j.gca.2018.05.006.

Chevrel, S.D., Pinet, P.C., Head, J.W., 1999. Gruithuisen domes region: a candidate for an extended nonmare volcanism unit on the Moon. J. Geophys. Res.: Planet. 104, 16515–16529. https://doi.org/10.1029/1998JE900007.

Cronberger, K., Neal, C.R., 2019. KREEP basalt 15382: not as pristine as originally thought. In: 50th Annual Lunar and Planetary Science Conference, p. 2444.

Cronberger, K., Neal, C.R., 2017. KREEP basalt petrogenesis: insights from 15434,181. Meteorit. Planet. Sci. 52, 827–841. https://doi.org/10.1111/maps.12837.

de Vries, J., van den Berg, A., van Westrenen, W., 2010. Formation and evolution of a lunar core from ilmenite-rich magma ocean cumulates. Earth Planet. Sci. Lett. 292, 139–147.

Dixon, S., Rutherford, M.J., 1979. Plagiogranites as late-stage immiscible liquids in ophiolite and mid-ocean ridge suites: an experimental study. Earth Planet. Sci. Lett. 45, 45–60.

Dowty, S., Keil, K., Prinz, M., Gros, J., Takahashi, H., 1976. Meteorite-free Apollo 15 crystalline KREEP. In: Lunar Science Conference, 7th, Houston, Tex., March 15-19, 1976, Proceedings, 2. Pergamon Press, Inc., New York, pp. 1833–1844, 1976pp. 1833–1844.

Drake, M.J., McCallum, I.S., McKay, G.A., Weill, D.F., 1970. Mineralogy and petrology of Apollo 12 sample no. 12013: a progress report. Earth Planet. Sci. Lett. 9, 103–123. Dygert, N., Hirth, G., Liang, Y., 2016. A flow law for ilmenite in dislocation creep: implications for lunar cumulate mantle overturn. Geophys. Res. Lett. 43, 532–540.

Elardo, S.M., Draper, D.S., Shearer Jr, C.K., 2011. Lunar Magma Ocean crystallization revisited: bulk composition, early cumulate mineralogy, and the source regions of the highlands Mg-suite. Geochim. Cosmochim. Acta 75, 3024–3045.

Elardo, S.M., Laneuville, M., McCubbin, F.M., Shearer, C.K., 2020. Early crust building enhanced on the Moon's nearside by mantle melting-point depression. Nat. Geosci. 13, 339–343. https://doi.org/10.1038/s41561-020-0559-4.

Elkins-Tanton, L.T., 2012. Magma oceans in the inner solar system. Annu. Rev. Earth. Planet. Sci. 40, 113–139.

Elkins-Tanton, L.T., Burgess, S., Yin, Q.-Z., 2011. The lunar magma ocean: reconciling the solidification process with lunar petrology and geochronology. Earth Planet. Sci. Lett. 304, 326–336.

Elkins-Tanton, L.T., Van Orman, J.A., Hager, B.H., Grove, T.L., 2002. Re-examination of the lunar magma ocean cumulate overturn hypothesis: melting or mixing is required. Earth Planet. Sci. Lett. 196, 239–249.

Elphic, R.C., Lawrence, D.J., Feldman, W.C., Barraclough, B.L., Maurice, S., Binder, A.B., Lucey, P.G., 2000. Lunar rare earth element distribution and ramifications for FeO and TiO2: lunar Prospector neutron spectrometer observations. J. Geophys. Res.: Planet. 105, 20333–20345.

Published in : Earth and Planetary Science Letters (2024), vol. 646, 118989
DOI: 10.1016/j.epsl.2024.118989
Status : Postprint (Author's version)

Gaffney, A.M., Borg, L.E., 2014. A young solidification age for the lunar magma ocean. Geochim. Cosmochim. Acta 140, 227–240.

Ghiorso, M.S., Carmichael, I.S.E., 1980. A regular solution model for met-aluminous silicate liquids: applications to geothermometry, immiscibility, and the source regions of basic magmas. Contr. Mineral. and Petrol. 71, 323–342. https://doi.org/ 10.1007/BF00374706.

Glotch, T.D., Hagerty, J.J., Lucey, P.G., Hawke, B.R., Giguere, T.A., Arnold, J.A., Williams, J.-P., Jolliff, B.L., Paige, D.A., 2011. The Mairan domes: silicic volcanic constructs on the Moon. Geophys. Res. Lett. 38.

Glotch, T.D., Lucey, P.G., Bandfield, J.L., Greenhagen, B.T., Thomas, I.R., Elphic, R.C., Bowles, N.E., Wyatt, M.B., Allen, C.C., Donaldson Hanna, K.L., 2010. Identification of highly silicic features on the Moon. In: 41st Annual Lunar and Planetary Science Conference, p. 1780.

Greenwood, J.P., Sakamoto, N., Itoh, S., Warren, P.H., Singer, J.A., Yanai, K., Yurimoto, H., 2017. The lunar magma ocean volatile signature recorded in chlorinerich glasses in KREEP basalts 15382 and 15386. Geochem. J. 51, 105–114.

Gullikson, A.L., Hagerty, J.J., Reid, M.R., Rapp, J.F., Draper, D.S., 2016. Silicic lunar volcanism: testing the crustal melting model. Am. Mineralog. 101, 2312–2321.

Hagerty, J.J., Lawrence, D.J., Hawke, B.R., Vaniman, D.T., Elphic, R.C., Feldman, W.C., 2006. Refined thorium abundances for lunar red spots: implications for evolved, nonmare volcanism on the Moon. J. Geophys. Res.: Planet. 111.

Herbert, F., 1980. Time-dependent lunar density models. In: Lunar and Planetary Science Conference Proceedings, pp. 2015–2030.

Hess, P.C., 2000. Petrogenesis of lunar troctolites-Implications for the Moon and its evolution. In: Lunar and Planetary Science Conference, p. 1389.

Hess, P.C., Parmentier, E.M., 2001. Thermal evolution of a thicker KREEP liquid layer. J. Geophys. Res.: Planet. 106, 28023–28032.

Hess, P.C., Parmentier, E.M., 1995. A model for the thermal and chemical evolution of the Moon's interior: implications for the onset of mare volcanism. Earth Planet. Sci. Lett. 134, 501–514.

Hess, P.C., Rutherford, M.J., Campbell, H.W., 1978. Ilmenite crystallization in nonmare basalt-Genesis of KREEP and high-Ti mare basalt. In: Lunar and Planetary Science Conference Proceedings, pp. 705–724.

Hess, P.C., Rutherford, M.J., Guillemette, R.N., Ryerson, F.J., Tuchfeld, H.A., 1975. Residual products of fractional crystallization of lunar magmas-an experimental study. In: Lunar and Planetary Science Conference Proceedings, pp. 895–909.

Honour, V.C., Holness, M.B., Partridge, J.L., Charlier, B., 2019. Microstructural evolution of silicate immiscible liquids in ferrobasalts. Contrib. Mineral Petrol. 174, 77. https://doi.org/10.1007/s00410-019-1610-6.

Published in : Earth and Planetary Science Letters (2024), vol. 646, 118989
DOI: 10.1016/j.epsl.2024.118989
Status : Postprint (Author's version)

Hou, T., Charlier, B., Holtz, F., Veksler, I., Zhang, Z., Thomas, R., Namur, O., 2018. Immiscible hydrous Fe–Ca–P melt and the origin of iron oxide-apatite ore deposits. Nat. Commun. 9, 1415. https://doi.org/10.1038/s41467-018-03761-4.

Hou, T., Charlier, B., Namur, O., Schütte, P., Schwarz-Schampera, U., Zhang, Z., Holtz, F., 2017. Experimental study of liquid immiscibility in the Kiruna-type Vergenoeg iron–fluorine deposit, South Africa. Geochim. Cosmochim. Acta 203, 303–322. https://doi.org/10.1016/j.gca.2017.01.025.

Hughes, S.S., Delano, J.W., Schmitt, R.A., 1988. Apollo 15 yellow-brown volcanic glass: chemistry and petrogenetic relations to green volcanic glass and olivine-normative mare basalts. Geochim. Cosmochim. Acta 52, 2379–2391.

Hui, H., Zhang, Y., 2007. Toward a general viscosity equation for natural anhydrous and hydrous silicate melts. Geochim. Cosmochim. Acta 71, 403–416.

Irving, A.J., 1977. Chemical Variation and Fractionation of KREEP Basalt Magmas. Pergamon Press.

Jerde, E.A., Snyder, G.A., Taylor, L.A., Yun-Gang, L., Schmitt, R.A., 1994. The origin and evolution of lunar high-Ti basalts: periodic melting of a single source at Mare Tranquillitatis. Geochim. Cosmochim. Acta 58, 515–527.

Jin, Z., Hou, T., Zhu, M.H., Zhang, Y., Namur, O., 2024. Late-stage microstructures in Chang'E-5 basalt and implications for the evolution of lunar ferrobasalt. Am. Mineral. https://doi.org/10.2138/am-2024-9448.

Jing, J.-J., Lin, Y., Knibbe, J.S., van Westrenen, W., 2022. Garnet stability in the deep lunar mantle: constraints on the physics and chemistry of the interior of the Moon. Earth Planet. Sci. Lett. 584, 117491 https://doi.org/10.1016/j.epsl.2022.117491.

Jolliff, B.L., 1998. Large-scale separation of K-frac and REEP-frac in the source regions of Apollo impact-melt breccias, and a revised estimate of the KREEP composition. Int. Geol. Rev. 40, 916–935.

Jolliff, B.L., 1991. Fragments of quartz monzodiorite and felsite in Apollo 14 soil particles. In: IN: Lunar and Planetary Science Conference, 21st. Lunar and Planetary Institute, Houston, TX, pp. 101–118. Houston, TX, Mar. 12-16, 1990, Proceedings (A91-42332 17-91)1991pp. 101–118.

Jolliff, B.L., Gillis, J.J., Haskin, L.A., Korotev, R.L., Wieczorek, M.A., 2000. Major lunar crustal terranes: surface expressions and crust-mantle origins. J. Geophys. Res.: Planet. 105, 4197–4216.

Jolliff, B.L., Wiseman, S.A., Lawrence, S.J., Tran, T.N., Robinson, M.S., Sato, H., Hawke, B.R., Scholten, F., Oberst, J., Hiesinger, H., 2011. Non-mare silicic volcanism on the lunar farside at Compton–Belkovich. Nat. Geosci. 4, 566–571.

Kesson, S.E., Ringwood, A.E., 1976. Mare basalt petrogenesis in a dynamic moon. Earth Planet. Sci. Lett. 30, 155–163.

Kleine, T., Palme, H., Mezger, K., Halliday, A.N., 2005. Hf-W chronometry of lunar metals and the age and early differentiation of the Moon. Science (1979) 310, 1671–1674.

Published in : Earth and Planetary Science Letters (2024), vol. 646, 118989
DOI: 10.1016/j.epsl.2024.118989
Status : Postprint (Author's version)

Knibbe, J.S., van Westrenen, W., 2015. The interior configuration of planet Mercury constrained by moment of inertia and planetary contraction. J. Geophys. Res.: Planet. 120, 1904–1923. https://doi.org/10.1002/2015JE004908.

Korotev, R.L., 2000. The great lunar hot spot and the composition and origin of the Apollo mafic ("LKFM") impact-melt breccias. J. Geophys. Res.: Planet. 105, 4317–4345.

Kraettli, G., Schmidt, M.W., Liebske, C., 2022. Fractional crystallization of a basal lunar magma ocean: a dense melt-bearing garnetite layer above the core? Icarus 371, 114699. https://doi.org/10.1016/j.icarus.2021.114699.

Krawczynski, M.J., Grove, T.L., 2012. Experimental investigation of the influence of oxygen fugacity on the source depths for high titanium lunar ultramafic magmas. Geochim. Cosmochim. Acta 79, 1–19.

Kress, V.C., Carmichael, I.S., 1991. The compressibility of silicate liquids containing Fe 2 O 3 and the effect of composition, temperature, oxygen fugacity and pressure on their redox states. Contribut. Mineral. Petrol. 108, 82–92.

Laneuville, M., Wieczorek, M.A., Breuer, D., Tosi, N., 2013. Asymmetric thermal evolution of the Moon. J. Geophys. Res.: Planet. 118, 1435–1452.

Lange, R.L., Carmichael, I.S., 1990. Thermodynamic properties of silicate liquids with emphasis on density, thermal expansion and compressibility. Rev. Mineral. Geochem. 24, 25–64.

Li, H., Zhang, N., Liang, Y., Wu, B., Dygert, N.J., Huang, J., Parmentier, E.M., 2019. Lunar cumulate mantle overturn: a model constrained by ilmenite rheology. J. Geophys. Res.: Planet. 124, 1357–1378.

Lin, Y., Shen, W., Liu, Y., Xu, L., Hofmann, B.A., Mao, Q., Tang, G.Q., Wu, F., Li, X.H., 2012. Very high-K KREEP-rich clasts in the impact melt breccia of the lunar meteorite SaU 169: new constraints on the last residue of the Lunar Magma Ocean. Geochim. Cosmochim. Acta 85, 19–40.

Lin, Y., Tronche, E.J., Steenstra, E.S., van Westrenen, W., 2017a. Evidence for an early wet Moon from experimental crystallization of the lunar magma ocean. Nat. Geosci. 10, 14–18.

Lin, Y., Tronche, E.J., Steenstra, E.S., van Westrenen, W., 2017b. Experimental constraints on the solidification of a nominally dry lunar magma ocean. Earth Planet. Sci. Lett. 471, 104–116.

Longhi, J., 2006. Petrogenesis of picritic mare magmas: constraints on the extent of early lunar differentiation. Geochim. Cosmochim. Acta 70, 5919–5934.

Longhi, J., 1990. Silicate liquid immiscibility in isothermal crystallization experiments. In: Lunar and Planetary Science Conference Proceedings, pp. 13–24.

Longhi, J., Walker, D., Grove, T.L., Stolper, E., Hays, J.F., 1974. The petrology of the Apollo 17 mare basalts. In: Lunar Science Conference, 5th, Houston, Tex., March 1822, 1974, Proceedings, 1. New York, Pergamon Press, Inc., pp. 447–469, 1974Research Supported by Harvard University; pp. 447–469.

Published in : Earth and Planetary Science Letters (2024), vol. 646, 118989
DOI: 10.1016/j.epsl.2024.118989
Status : Postprint (Author's version)

Maurice, M., Tosi, N., Hüttig, C., 2024. Small-scale overturn of high-Ti cumulates promoted by the long lifetime of the lunar magma ocean. J. Geophys. Res.: Planet. 129, e2023JE008060.

McCubbin, F.M., Jolliff, B.L., Nekvasil, H., Carpenter, P.K., Zeigler, R.A., Steele, A., Elardo, S.M., Lindsley, D.H., 2011. Fluorine and chlorine abundances in lunar apatite: implications for heterogeneous distributions of magmatic volatiles in the lunar interior. Geochim. Cosmochim. Acta 75, 5073–5093.

McCubbin, F.M., Vander Kaaden, K.E., Tartese, R., Boyce, J.W., Mikhail, S., Whitson, E.` S., Bell, A.S., Anand, M., Franchi, I.A., Wang, J., Hauri, E.H., 2015. Experimental investigation of F, Cl, and OH partitioning between apatite and Fe-rich basaltic melt at 1.0–1.2 GPa and 950–1000 ◦C. Am. Mineralog. 100, 1790–1802. https://doi.org/ 10.2138/am-2015-5233.

McKay, G.A., Wiesmann, H., Bansal, B.M., Shih, C.-Y., 1979. Petrology, chemistry, and chronology of Apollo 14 KREEP basalts. In: Lunar and Planetary Science Conference Proceedings, pp. 181–205.

McKay, G.A., Wiesmann, H., Nyquist, L.E., Wooden, J.L., Bansal, B.M., 1978. Petrology, chemistry, and chronology of 14078-Chemical constraints on the origin of KREEP. In: Lunar and Planetary Science Conference, 9th, Houston, Tex., March 13-17, 1978, Proceedings, 1. Pergamon Press, Inc., New York, pp. 661–687, 1978pp. 661–687.

McKenzie, D., 2011. Compaction and crystallization in magma chambers: towards a model of the skaergaard intrusion. J. Petrol. 52, 905–930. https://doi.org/10.1093/ petrology/egr009.

Neal, C.R., Donohue, P., Fagan, A.L., O'Sullivan, K., Oshrin, J., Roberts, S., 2015. Distinguishing between basalts produced by endogenic volcanism and impact processes: a non-destructive method using quantitative petrography of lunar basaltic samples. Geochim. Cosmochim. Acta 148, 62–80. https://doi.org/10.1016/j. gca.2014.08.020.

Neal, C.R., Taylor, L.A., 1989. Metasomatic products of the lunar magma ocean: the role of KREEP dissemination. Geochim. Cosmochim. Acta 53, 529–541.

Nyquist, L.E., 1977. Lunar Rb-Sr chronology. Physics and Chemistry of the Earth 10.

Nyquist, L.E., Hubbard, N.J., Gast, P.W., Bansal, B.M., Weismann, H., Jahn, B., 1973. RbSr systematics for chemically defined Apollo 15 and 16 materials. In: Proceedings of the Lunar Science Conference, 4, p. 1823, p. 1823.

O'Neill, H.S.C., 1991. The origin of the Moon and the early history of the Earth-a chemical model. Part 1: The Moon. Geocheim. Cosmochim. Acta 55, 1135–1157.

Parmentier, E.M., Zhong, S., Zuber, M.T., 2002. Gravitational differentiation due to initial chemical stratification: origin of lunar asymmetry by the creep of dense KREEP? Earth Planet. Sci. Lett. 201, 473–480.

Pernet-Fisher, J.F., Howarth, G.H., Liu, Y., Chen, Y., Taylor, L.A., 2014. Estimating the lunar mantle water budget from phosphates: complications associated with silicateliquid-immiscibility. Geochim. Cosmochim. Acta 144, 326–341.

Prissel, K.B., Krawczynski, M.J., Nie, N.X., Dauphas, N., Aarons, S.M., Heard, A.W., Hu, M.Y., Alp, E.E., Zhao, J., 2024. Fractionation of iron and titanium isotopes by ilmenite and the isotopic compositions

Published in : Earth and Planetary Science Letters (2024), vol. 646, 118989
DOI: 10.1016/j.epsl.2024.118989
Status : Postprint (Author's version)

of lunar magma ocean cumulates. Geochimica et Cosmochimica Acta S0016703724000164. https://doi.org/10.1016/ j.gca.2024.01.006.

Qian, Y., She, Z., He, Q., Xiao, L., Wang, Z., Head, J.W., Sun, L., Wang, Y., Wu, B., Wu, X., 2023. Mineralogy and chronology of the young mare volcanism in the ProcellarumKREEP-Terrane. Nat. Astron. 7, 287–297.

Rapp, J.F., Draper, D.S., 2018. Fractional crystallization of the lunar magma ocean: updating the dominant paradigm. Meteorit. Planet. Sci. 53, 1432–1455.

Ringwood, A.E., Kesson, S.E., 1976. A dynamic model for mare basalt petrogenesis. In: Lunar Science Conference, 7th, Houston, Tex., March 15-19, 1976, Proceedings, 2.

Pergamon Press, Inc., New York, pp. 1697–1722, 1976pp. 1697–1722.

Rivoldini, A., Van Hoolst, T., Verhoeven, O., 2009. The interior structure of Mercury and its core sulfur content. Icarus 201, 12–30.

Robinson, K.L., Barnes, J.J., Nagashima, K., Thomen, A., Franchi, I.A., Huss, G.R., Anand, M., Taylor, G.J., 2016. Water in evolved lunar rocks: evidence for multiple reservoirs. Geochim. Cosmochim. Acta 188, 244–260.

Roedder, E., Weiblen, P.W., 1970. Silicate liquid immiscibility in lunar magmas, evidenced by melt inclusions in lunar rocks. Science (1979) 167, 641–644.

Rutherford, M.J., Hess, P.C., Daniel, G.H., 1974. Experimental liquid line of descent and liquid immiscibility for basalt 70017. In: Lunar and Planetary Science Conference Proceedings, pp. 569–583.

Ryder, G., 1988. Quenching and disruption of lunar KREEP lava flows by impacts. Nature 336, 751–754.

Ryder, G., 1987. Petrographic evidence for nonlinear cooling rates and a volcanic origin for Apollo 15 KREEP basalts. J. Geophys. Res.: Solid Earth 92, E331–E339.

Ryder, G., Bower, J.F., 1976. Poikilitic KREEP impact melts in the Apollo 14 white rocks. In: Lunar Science Conference, 7th, Houston, Tex., March 15-19, 1976, Proceedings, 2. Pergamon Press, Inc., New York, pp. 1925–1948, 1976pp. 1925–1948.

Ryder, G., Stoeser, D.B., Wood, J.A., 1977. Apollo 17 KREEPy basalt: a rock type intermediate between mare and KREEP basalts. Earth Planet. Sci. Lett. 35, 1–13.

Ryerson, F.J., Hess, P.C., 1980. The role of P2O5 in silicate melts. Geochim. Cosmochim. Acta 44, 611–624.

Ryerson, F.J., Hess, P.C., 1978. Implications of liquid-liquid distribution coefficients to mineral-liquid partitioning. Geochim. Cosmochim. Acta 42, 921–932.

Schmidt, M.W., Connolly, J.A.D., Gunther, D., Bogaerts, M., 2006. Element partitioning: the role of melt structure and composition. Science (1979) 312, 1646–1650.

Schmidt, M.W., Kraettli, G., 2022. Experimental crystallization of the Lunar Magma Ocean, initial selenotherm and density stratification, and implications for crust formation, overturn and the bulk

Published in : Earth and Planetary Science Letters (2024), vol. 646, 118989
DOI: 10.1016/j.epsl.2024.118989
Status : Postprint (Author's version)

silicate moon composition. J. Geophys. Res.: Planet. 127, e2022JE007187 https://doi.org/10.1029/2022JE007187.

Seddio, S.M., Jolliff, B.L., Korotev, R.L., Zeigler, R.A., 2013. Petrology and geochemistry of lunar granite 12032, 366-19 and implications for lunar granite petrogenesis. Am. Mineralog. 98, 1697–1713.

Shearer, C.K., Papike, J.J., 2005. Early crustal building processes on the moon: models for the petrogenesis of the magnesian suite. Geochim. Cosmochim. Acta 69, 3445–3461.

Shervais, J.W., McGee, J.J., 1998. Ion and electron microprobe study of troctolites, norite, and anorthosites from Apollo 14: evidence for urKREEP assimilation during petrogenesis of Apollo 14 Mg-suite rocks. Geochim. Cosmochim. Acta 62, 3009–3023.

Edited by Smith, J.V., Anderson, A.T., Newton, R.C., Olsen, E.J., Crewe, A.V., Isaacson, M.S., Johnson, D., Wyllie, P.J., 1970. Petrologic history of the moon inferred from petrography, mineralogy and petrogenesis of Apollo 11 rocks. In: Levinson, AA (Ed.), Geochimica et Cosmochimica Acta Supplement, Volume 1. Proceedings of the Apollo 11 Lunar Science Conference Held 5-8 January 1970 in Houston, TX. Volume 1: Mineraolgy and Petrology. Pergammon Press, New York, p. 897. Edited by1970p. 897.

Snyder, G.A., Taylor, L.A., Neal, C.R., 1992. A chemical model for generating the sources of mare basalts: combined equilibrium and fractional crystallization of the lunar magmasphere. Geochim. Cosmochim. Acta 56, 3809–3823. https://doi.org/ 10.1016/0016-7037(92)90172-F.

Solomatov, V., 2007. Magma oceans and primordial mantle differentiation. Evolut. Earth 9, 91–119.

Solomon, S.C., Longhi, J., 1977. Magma oceanography. I-thermal evolution. In: Lunar and Planetary Science Conference Proceedings, pp. 583–599.

Taylor, G.J., Warner, R.D., Keil, K., Ma, M.-S., Schmitt, R.A., 1980. Silicate liquid immiscibility, evolved lunar rocks and the formation of KREEP. Lunar Highlands Crust, pp. 339–352.

Taylor, S.R., 1982. Planetary Science: A lunar Perspective. Lunar and Planetary Institute, Houston, p. 502.

Taylor, S.R., Jakeˇs, P., 1974. The Geochemical Evolution of the Moon. Pergamon Press. Tian, H.-C., Wang, H., Chen, Y., Yang, W., Zhou, Q., Zhang, C., Lin, H.-L., Huang, C., Wu, S.-T., Jia, L.-H., Xu, L., Zhang, D., Li, X.-G., Chang, R., Yang, Y.-H., Xie, L.-W., Zhang, D.-P., Zhang, G.-L., Yang, S.-H., Wu, F.-Y., 2021. Non-KREEP origin for Chang'e-5 basalts in the Procellarum KREEP Terrane. Nature 600, 59–63. https:// doi.org/10.1038/s41586-021-04119-5.

Tonks, W.B., Melosh, H.J., 1993. Magma ocean formation due to giant impacts. J. Geophys. Res.: Planet. 98, 5319–5333.

Tosi, N., Padovan, S., 2021. Mercury, Moon, Mars: Surface Expressions of Mantle Convection and Interior Evolution of Stagnant-Lid Bodies. Mantle Convection and Surface Expressions, pp. 455–489.

Veksler, I.V., Dorfman, A.M., Danyushevsky, L.V., Jakobsen, J.K., Dingwell, D.B., 2006. Immiscible silicate liquid partition coefficients: implications for crystal-melt element partitioning and basalt petrogenesis. Contribut. Mineral. Petrol. 152, 685–702.

Published in : Earth and Planetary Science Letters (2024), vol. 646, 118989
DOI: 10.1016/j.epsl.2024.118989
Status : Postprint (Author's version)

Warren, P.H., 1988. The origin of pristine KREEP-Effects of mixing between UrKREEP and the magmas parental to the Mg-rich cumulates. In: Lunar and Planetary Science Conference Proceedings, pp. 233–241.

Warren, P.H., 1985. The magma ocean concept and lunar evolution. In: IN: Annual review of Earth and Planetary Sciences, 13. Annual Reviews, Inc., Palo Alto, CA, pp. 201–240, 198513, 201–240.

Warren, P.H., Jerde, E.A., Kallemeyn, G.W., 1987. Pristine Moon rocks: a "large" felsite and a metal-rich ferroan anorthosite. J. Geophys. Res.: Solid Earth 92, E303–E313.

Warren, P.H., Taylor, G.J., Keil, K., Shirley, D.N., Wasson, J.T., 1983. Petrology and chemistry of two "large" granite clasts from the moon. Earth Planet. Sci. Lett. 64, 175–185. https://doi.org/10.1016/0012-821X(83)90202-9.

Warren, P.H., Wasson, J.T., 1979. The origin of KREEP. Rev. Geophys. 17, 73–88. https://doi.org/10.1029/RG017i001p00073.

Watson, E.B., 1976. Two-liquid partition coefficients: experimental data and geochemical implications. Contribut. Mineral. Petrol. 56, 119–134.

Wieczorek, M.A., Neumann, G.A., Nimmo, F., Kiefer, W.S., Taylor, G.J., Melosh, H.J., Phillips, R.J., Solomon, S.C., Andrews-Hanna, J.C., Asmar, S.W., Konopliv, A.S., Lemoine, F.G., Smith, D.E., Watkins, M.M., Williams, J.G., Zuber, M.T., 2013. The Crust of the Moon as Seen by GRAIL. Science (1979) 339, 671–675. https://doi.org/ 10.1126/science.1231530.

Wieczorek, M.A., Phillips, R.J., 2000. The "Procellarum KREEP Terrane": implications for mare volcanism and lunar evolution. J. Geophys. Res.: Planet. 105, 20417–20430.

Edited by Wood, J.A., Dickey Jr, J.S., Marvin, U.B., Powell, B.N., 1970. Lunar anorthosites and a geophysical model of the moon. In: Levinson, AA (Ed.), Geochimica et Cosmochimica Acta Supplement, Volume 1. Proceedings of the Apollo 11 Lunar Science Conference Held 5-8 January 1970 in Houston, TX. Volume 1: Mineralogy and Petrology. Pergammon Press, New York, p. 965. Edited by1970p. 965.

Xu, M., Jing, Z., Van Orman, J.A., Yu, T., Wang, Y., 2022. Experimental Evidence Supporting an Overturned Iron-Titanium-Rich Melt Layer in the Deep Lunar Interior. Geophys. Res. Lett. 49, e2022GL099066.

Yu, S., Tosi, N., Schwinger, S., Maurice, M., Breuer, D., Xiao, L., 2019. Overturn of ilmenite-bearing cumulates in a rheologically weak lunar mantle. J. Geophys. Res.: Planet. 124, 418–436.

Zhang, A.-C., Taylor, L.A., Wang, R.-C., Li, Q.-L., Li, X.-H., Patchen, A.D., Liu, Y., 2012. Thermal history of Apollo 12 granite and KREEP-rich rock: clues from Pb/Pb ages of zircon in lunar breccia 12013. Geochim. Cosmochim. Acta 95, 1–14.

Zhang, N., Ding, M., Zhu, M.-H., Li, Huacheng, Li, Haoyuan, Yue, Z., 2022. Lunar compositional asymmetry explained by mantle overturn following the South Pole–Aitken impact. Nat. Geosci. 15, 37–41.

Published in : Earth and Planetary Science Letters (2024), vol. 646, 118989
DOI: 10.1016/j.epsl.2024.118989
Status : Postprint (Author's version)

Zhang, N., Dygert, N., Liang, Y., Parmentier, E.M., 2017. The effect of ilmenite viscosity on the dynamics and evolution of an overturned lunar cumulate mantle. Geophys. Res. Lett. 44, 6543–6552.

Zhang, Y., Namur, O., Charlier, B., 2023. Experimental study of high-Ti and low-Ti basalts: liquid lines of descent and silicate liquid immiscibility in large igneous provinces. Contribut. Mineral. Petrol. 178, 7.